The Spectrum of IDH- and H3-Wildtype High-Grade Glioma Subgroups Occurring across Teenage and Young Adult Patient Populations

Rita Pereira[1], Alan Mackay[1], Yura Grabovska[1], Amelia Bradley[2], Tabitha Bloom[2], James Nicoll[2], Delphine Boche[2], John Procter[3], Mellissa Maybury[4,5], Johanna Schagen[5], Liam Walker[6,7], Federico Roncaroli[6,7], Konstantina Karabatsou[8], Olumide Ogunbiyi[9], Thijs van Dalen[10], Jai Sidpra[11], Sabrina Rossi[12], Evelina Miele[13], David S. Ziegler[14,15,16], Zhifeng Shi[17], Thomas S. Jacques[7], Darren Hargrave[11], Bassel Zebian[18], Cristina Bleil[18], Joseph Yates[19], Emma Norton[19], Henry Mandeville[20,21], Antonia Creak[21,22], Liam Welsh[21,22], Lynley Marshall[20,21,23], Fernando Carceller[20,21], Sucheta J. Vaidya[20,21], Zita Reisz[24], Safa Al-Sarraj[24], Angela Mastronuzzi[25], Andrea Carai[26], Maria Vinci[27], Kathreena M. Kurian[28], Ho-keung Ng[29], Sebastian Brandner[30], Chris Jones[1], and Matthew Clarke[1,30]

ABSTRACT

Purpose: High-grade gliomas (HGG) occur in any central nervous system location and at any age. HGGs in teenagers/young adults (TYA) are understudied. This project aimed to characterize these tumors to support accurate stratification of patients.

Experimental Design: 207 histone/IDH wild-type tumors from patients aged 13 to 30 years were collected. DNA methylation profiling [Illumina EPIC BeadArrays, brain tumor classifier (MNPv12.8 R package)] classified cases against reference cohorts of HGG. Calibrated scores guided characterization workflows [RNA-based ArcherDx fusion panel ($n = 92$), whole-exome sequencing ($n = 107$), and histology review).

Results: 53.4% ($n = 86$) matched as pediatric-type subgroups [pedHGG_RTK1A/B/C (31.7%, $n = 51$, *PDGFRA*, *CDKN2A/B*, *SETD2*, and *NF1* alterations), pedHGG_*MYCN* (8.1%, $n = 13$, *MYCN/ID2* amplifications), and pedHGG_RTK2A/B (7.5%, $n = 12$, *TP53*, *BCOR*, *ATRX*, and *EGFR* alterations)]. Eighteen percent ($n = 29$) classified as adult-type subgroups [GBM_MES (15.5%, $n = 25$, enriched for *RB1*, *PTEN*, and *NF1* alterations) and GBM_RTK1/2 (2.5%, $n = 4$, *CDK4* amplifications)]. Twenty-three cases (14.7%) classified as novel, poorly characterized subgroups with distinct methylation profiles and molecular features [pedHGG_A/B ($n = 10$ 6.2%), HGG_E ($n = 6$ 3.7%), HGG_B ($n = 2$ 1.0%), and GBM_CBM ($n = 5$ 3.1%)] with variable histologic morphology. Eight cases (5.1%) showed hypermutator phenotypes, enriched in HGG_E, one of which was associated with constitutional mismatch repair deficiency, and their sibling, who was diagnosed with the same syndrome, was diagnosed with a tumor that classified as a pedHGG_RTK1B. HGGs that have developed on a background of previous treatment for a childhood cancer are detected in the TYA population, classifying most frequently as pedHGG_RTK1 and contributing to the poor prognosis of this subgroup. Age distribution/molecular profile comparisons using publicly available methylation/sequencing data (and from local diagnostic cohorts) for HGG_B ($n = 19$), GBM_CBM ($n = 35$), and GBM_MES_ATYP ($n = 102$), irrespective of age, show that HGG_B is a TYA-specific subgroup (median age 29 years) and that GBM_CBM and GBM_MES_ATYP show a peak of distribution in the TYA population but also have a wider age distribution (median age 35.7 and 50.5 years, respectively), with the latter showing distinct differences in copy-number profiles compared with older adults in the same subgroup and containing fewer chr7 gains, chr10 losses, more *CDKN2A/B* deletions and *MET* amplifications, and a worse survival compared with adult-specific GBM_MES_TYP.

Conclusions: TYA HGGs comprise novel methylation subgroups with distinct methylation and molecular profiles. Accurate stratification of these patients will open opportunities to more effective treatments, including immune checkpoint, MAPK pathway, and *PDGFRA* inhibitors.

See related commentary by Ritzmann et al., p. 3110

Introduction

High-grade gliomas (HGG) comprise different subgroups of aggressive central nervous system (CNS) tumors in both adults and children, including infants (1, 2). They can occur in any CNS location (3, 4) within the cranio–spinal axis and have a poor prognosis (20.8% 5-year survival for those diagnosed between 0 and 19 years and 21.9% for patients aged 20–44 years; refs. 3, 5). Outcomes are considerably better than those of older adults, with patients aged 45 to 54 and 55 to 64 years having a 5-year survival of

[1]Division of Molecular Pathology, Institute of Cancer Research, London, United Kingdom. [2]Clinical Neurosciences, Clinical and Experimental Sciences, Faculty of Medicine, University of Southampton, Southampton, United Kingdom. [3]Neuropathology and Pathology Research, Royal Preston Hospital, Preston, United Kingdom. [4]Oncology Services Group, Queensland Children' Hospital, Brisbane, Australia. [5]Child Health Research Centre, The University of Queensland, Brisbane, Australia. [6]Department of Cellular Pathology, Northern Care Alliance, Salford, United Kingdom. [7]Geoffrey Jefferson Brain Research Centre, Division of Neuroscience, School of Biology, University of Manchester, Manchester, United Kingdom. [8]Department of Neurosurgery, Manchester Centre of Clinical Neuroscience, Northern Care Alliance, Salford, United Kingdom. [9]Neuropathology Department, Great Ormond Street Hospital for Children NHS Foundation Trust, London, United Kingdom. [10]Neurosurgery Department, National Hospital for Neurology and Neurosurgery, UCLH, London, United Kingdom. [11]Paediatric Neuro Oncology, UCL Great Ormond Street Institute of Child Health, London, United Kingdom.

Translational Relevance

High-grade gliomas (HGG) in teenagers and young adults (TYA) are an understudied group of tumors. Through national and international collaboration, we have gathered a large series of 207 cases for the purpose of molecular characterization using DNA methylation profiling, whole-exome sequencing, and fusion panel sequencing, alongside neuropathologic review. We integrate histopathology, genetic, and epigenetic profiling to present the spectrum of different subtypes of HGG that occur in the TYA population. We identify that HGGs occurring in TYAs comprise methylation subgroups that occur in pediatric and adult age groups but also novel, poorly defined methylation classes, which this study helps to characterize. The study highlights mutational landscapes that may be targetable with immune checkpoint, MAPK pathway, and *PDGFRA* inhibitors. Incidences of tumor predisposition syndromes (including constitutional mismatch repair disorder) are identified in the cohort, and we also identify tumors that have developed on a background of previous treatment for childhood cancers. These data also highlight the value of undertaking DNA methylation profiling and whole-exome/panel sequencing on each HGG occurring in the TYA age group to accurately diagnose and characterize these complex tumors.

9.3% and 5.9%, respectively, suggesting that underlying biology may differ (3). It remains a significant clinical and therapeutic challenge to understand more about the development, characteristics, and evolution of these tumors to advance therapeutic interventions and improve survival (6, 7).

DNA methylation profiling and the development of the Molecular Neuropathology (MNP) brain tumor classifier have transformed diagnostic practice (8, 9), providing a molecular tool supporting delivery of accurate diagnoses for challenging cases. Copy number profiles and prognostic information can be gained (9), and it provides opportunities to discover and characterize new tumor entities (8, 9) for more accurate patient stratification (10, 11).

The fifth edition of the World Health Organization (WHO) classification of tumors of the CNS now recognizes that high- and low-grade diffuse glial tumors occurring in adults and children comprise distinct entities with distinctive molecular profiles (12); histone-mutant CNS tumors (diffuse midline glioma, H3 K27-altered; diffuse hemispheric glioma, H3 G34-mutant) are considered pediatric-type HGGs (12, 13). The WHO classification also recognizes the newly defined pediatric entities, including the infant-type hemispheric glioma, seen predominantly in the infant population and characterized by distinct methylation profiles and RTK fusions (1, 2).

Approximately 60% of CNS tumors diagnosed in teenagers and young adults (TYA) each year in the United Kingdom will be a glial tumor (14), representing the fourth most frequent cancer type occurring in patients aged 15 to 24 years (12). They account for 60% of cancer-related deaths in this age range (14). This group denotes an understudied set of tumors with very limited published clinical, pathologic, and molecular data. No distinct HGG subgroups are recognized as TYA-specific according to the WHO classification (12). Studies have explored a variety of molecular-based techniques (IHC, targeted/next-generation sequencing, whole-exome sequencing (WES), and much less frequently epigenetic profiling) and show that a proportion of TYA HGGs can be classified into well-recognized HGG entities, including diffuse midline gliomas, H3 K27-altered, diffuse hemispheric glioma, H3 G34-mutant, and IDH-mutant HGGs (15, 16). However, other tumors remained unclassifiable (15). A meta-analysis of >1,000 pediatric HGGs and diffuse midline gliomas (DMG), including patients aged up to 35 years, identified diverse clinical and biological subgroups characterized by different somatic mutations (16) and showed that survival of TYA HGGs was significantly better compared with older adults and H3-mutant groups (16), suggesting that novel entities of HGG with differing underlying biology exist.

Gross total resection (GTR) is the mainstem HGG treatment, including for TYA patients. Given their infiltrative nature, residual and radiologically undetectable tumors frequently remain, leading to recurrence and progression. Postoperative chemotherapy and radiotherapy have considerable cumulative side effects (17–19), including impaired cognitive function (14). Studies have also shown very limited benefit for patients with

[12]Sabrina Rossi. Pathology Unit, Bambino Gesù Children's Hospital IRCCS, Rome, Italy. [13]Pediatric Onco-Haematology, Cell Therapy, Gene Therapies and Hematopoietic Transplant, Bambino Gesù Children's Hospital-IRCCS, Rome, Italy. [14]Children's Cancer Institute, Lowy Cancer Centre, UNSW Sydney, Kensington, Australia. [15]School of Clinical Medicine, UNSW Medicine & Health, UNSW Sydney, Kensington, Australia. [16]Kids Cancer Centre, Sydney Children's Hospital, Randwick, Australia. [17]Neurosurgery, Fudan University, Shanghai, China. [18]Neurosurgery Department, King's College Hospital, London, United Kingdom. [19]Department of Cellular Pathology, University Hospital Southampton NHS Trust, Southampton, United Kingdom. [20]Department of Paediatric and Teenager & Young Adult Neuro-Oncology, The Royal Marsden Hospital NHS Foundation Trust, London, United Kingdom. [21]Division of Clinical Studies, The Institute of Cancer Research, London, United Kingdom. [22]Department of Adult Neuro-Oncology, The Royal Marsden Hospital NHS Foundation Trust, London, United Kingdom. [23]Paediatric and Adolescent Oncology Drug Development Unit, The Royal Marsden NHS Foundation Trust, London, United Kingdom. [24]Neuropathology Department, King's College Hospital, London, United Kingdom. [25]Pediatric Onco-Hematology, Cell Therapy, Gene Therapies and Hematopoietic Transplant, Bambino Gesù Children's Hospital - IRCCS, Rome, Italy. [26]Neurosurgery Unit, Bambino Gesù Children's Hospital – IRCCS, Rome, Italy. [27]Paediatric Cancer Genetics and Epigenetics Research Unit, Bambino Gesù Children's Hospital-IRCCS, Rome, Italy. [28]University of Bristol Brain Tumour Research Centre, Neuropathology, Southmead Hospital, Bristol, United Kingdom. [29]Chinese University of Hong Kong, Hong Kong, China. [30]Division of Neuropathology, The National Hospital for Neurology and Neurosurgery, University College London Hospitals NHS Foundation Trust, and Queen Square Institute of Neurology, London, United Kingdom.

R. Pereira, A. Mackay, Y. Grabovska, C. Jones, and M. Clarke contributed equally to the article.

Corresponding Author: Matthew Clarke, Division of Molecular Pathology, Institute of Cancer Research, 15 Cotswold Road, Sutton, London SM2 5NG, United Kingdom. E-mail: matthew.clarke01@icr.ac.uk

Clin Cancer Res 2025;31:3259–75

doi: 10.1158/1078-0432.CCR-24-1256

HGG undergoing re-resection of residual tumor (20) and highlight the psychosocial impact of a brain tumor diagnosis for TYA patients (14). As efforts to improve survival continue, it remains imperative to minimize short- and long-term side-effect profiles or find more targeted alternatives better suited to these complex tumors.

In this study, we have investigated a series of TYA HGGs integrating DNA methylation, mutational analysis, and neuropathologic and clinical annotations and identified novel tumor subgroups with distinctive methylation profiles.

Materials and Methods

Cases

A total of 398 samples were collected from national and international collaborators (tumor samples: University College London Hospitals, London, $n = 63$; internal biobank, $n = 58$; King's College Hospital, London, $n = 39$; Southampton General Hospital, $n = 38$; The Chinese University of Hong Kong, $n = 37$; Salford NHS Foundation Trust, $n = 33$; Royal Preston Hospital $n = 29$; Bambino Gesù Children's Hospital, Rome, $n = 26$; Queensland Children's Tumor Bank, Brisbane, $n = 23$; University Hospitals Bristol, $n = 17$; Great Ormond Street Hospital, London, $n = 15$; Poland, $n = 11$; and Children's Cancer Institute and Sydney Children's Hospital, $n = 9$). Where possible, both formalin-fixed paraffin-embedded (FFPE) and/or frozen tissue samples were provided for each case. Data were also retrieved and integrated from previously published studies from the Jones Lab (2, 16, 21). Patients were selected according to age (≥13 to ≤30 years old) and diagnosis [IDH/H3 wild-type (WT) glioma, WHO grade 2, 3, or 4]. Definitions of TYA age are variable, with the United Kingdom stating that the age range is between 16 and 24 years (22); for this study, we decided to broaden the age to ≥13 to ≤30 years old to ensure the age distribution for each tumor subtype could be captured. Cases were excluded if they were diagnosed at the center of origin/classified as a well-characterized subtype of HGG according to the WHO 2021 (astrocytoma, IDH-mutant; diffuse midline glioma, H3 K27-altered; and diffuse hemispheric glioma, H3 G34-mutant). All CNS WHO grade 1 gliomas and glioneuronal tumor diagnoses were excluded, alongside non-gliomas (ependymal, embryonal, mesenchymal, and germ cell tumors). Tissue samples obtained from the University Hospital Southampton NHS Foundation Trust, Royal Preston Hospital, Great Ormond Street Institute for Child Health, University College London Hospitals, Southmead Hospital, and the Northern Care Alliance, as part of BRAIN UK, were supported by Brain Tumor Research, the British Neuropathological Society, and the Medical Research Council.

A final cohort of 207 samples was investigated.

Consent and ethics statement

Written informed consent was obtained for all samples included in this study under Research Ethics Committee approval at each participating center. Project specific Research Ethical Approval was also received via application to BRAIN UK (23).

Nucleic acid extraction

DNA and RNA were extracted from frozen tissue using *Quick*-DNA/RNA Miniprep Plus Kit (Zymo) according to the manufacturer's instructions. For FFPE tissue, DNA was extracted where possible after manual macrodissection using QIAamp DNA FFPE Tissue Kit protocol (QIAGEN), and RNA was extracted using All-Prep DNA/RNA kit (Qiagen) according to the manufacturer's instructions.

Methylation profiling

Analysis was performed using Illumina EPIC BeadArrays at University College London Great Ormond Street Institute of Child Health when more than 140 ng of DNA was extracted. Data from EPIC arrays were preprocessed using the minifi package in R (v1.48.0). 15 Italian cases were analyzed at Bambino Gesù Children's Hospital, and raw data were shared and included for the bioinformatic analyses. Data from EPIC arrays were preprocessed using the minifi package in R (v1.48.0). A cohort of 207 cases met the entry criteria and could progress into the study. The Heidelberg brain tumor classifier (molecularneuropathology.org) was used to assign a calibrated score to each case, associating it with one of the >100 tumor entities which feature within the classifier (v12.8). Tumors were subclassified into one of 17 methylation subgroups; diffuse pediatric-type HGG, H3 WT and IDH WT, subtype A/B (pedHGG_A/B), diffuse pediatric-type HGG, MYCN subtype (pedHGG_MYCN), diffuse pediatric-type HGG, RTK1 subtype, subclass A/B/C (pedHGG_RTK1A/B/C), diffuse pediatric-type HGG, RTK2 subtype, subclass A/B (pedHGG_RTK2A/B), glioblastoma, IDH WT, subtype posterior fossa (GBM_CBM), adult-type diffuse HGG, IDH WT, subtype E (HGG_E), adult-type diffuse HGG, IDH WT, subtype B (HGG_B), glioblastoma, IDH WT, RTK1 subtype (GBM_RTK1), glioblastoma, IDH WT, RTK2 subtype (GBM_RTK2), glioblastoma, IDH WT, mesenchymal subtype, typical/atypical (GBM_MES_TYP/ATYP), pleomorphic xanthoastrocytoma (PXA), and high-grade astrocytoma with piloid features (HGAP). Clustering of β values from methylation arrays was performed based upon correlation distance using a ward algorithm. Quality control (QC) was undertaken; the methylation data for samples in which the probe failure rate was >20% or bisulfite conversion failed were excluded from the methylation analysis. However, they were not excluded from the study and were analyzed with other workflow streams. Mean *P* value detection is a common QC filtering criteria and is advised by Illumina. However, the probe failure rate is not stringent because of the inclusion of historic FFPE cases. To date, Illumina do not provide specific guidelines on the cutoff and advise discretion. The MNP classifier uses 10,000 probes; cases with a probe failure rate ≤20% showed concordance with MNP assignments, t-statistic–based stochastic neighbor embedding (t-SNE) location, and clinical/genomic case annotations.

Samples were assigned a methylation subgroup when the calibrated score was >0.5 and after correlating with the histologic diagnosis and available molecular data. Samples with a calibrated score of <0.5, or if the assignment was not appropriate, were assigned as "not elsewhere classified," as per the WHO classification definition, and underwent further characterization to determine their subtype.

Reference cohorts

Classifier results for the TYA cohort were plotted against a t-SNE reference cohort of CNS tumors, composed of 8,488 pairs of publicly available methylation iDats for different brain tumor types that are part of the classifier (derived from accession numbers E-MTAB-3476, E-MTAB-4969, E-MTAB-5797, E-MTAB-7490, E-MTAB-8390, E-MTAB-8888, GSE103659, GSE104210, GSE104293, GSE109330, GSE109381, GSE116298, GSE117130, GSE119774, GSE122038, GSE122920, GSE122994, GSE123678, GSE124617, GSE125450,

GSE128654, GSE131482, GSE133801, GSE135017, GSE136361, GSE137845, GSE138221, GSE140124, GSE143843, GSE147391, GSE152653, GSE156012, GSE156090, GSE157397, GSE164994, GSE166569, GSE183656, GSE183972, GSE184900, GSE188547, GSE190362, GSE193196, GSE196490, GSE197378, GSE198855, GSE200647, GSE215240, GSE36278, GSE52556, GSE55712, GSE60274, GSE61160, GSE65362, GSE70460, GSE73801, GSE73895, GSE85218, GSE92577, and GSE92579), TCGA_GBM and TCGA_LGG. Entry into the reference cohort was determined by the same QC metrics as for the TYA cohort. Data were derived from 450K and 850K array data and were combined using combineArrays() functionality from minfi, reducing both arrays to their common set of probes. The reference cohort therefore comprised methylation profiles for the spectrum of different brain tumor types, irrespective of age, that the TYA methylation cohort could be compared with in terms of their t-SNE cluster locations and allowed the exclusion of any cases that classified or aligned with non-glial tumors. Gender information was available for 4,653 cases; 2,109 cases were from female patients, and 2,544 from male patients. Age was available for 5,078 cases (median 19 years, range 0.1–93 years). The glioma reference cohort was derived by filtering the CNS reference cohort for the different glial subtypes (specifically high-grade glial tumors). Cohorts of all the existing HGG entities that are currently part of the v12.8 classifier were represented. Gender information was available for 1,446 cases (604 female and 842 male). Age was available for 1,434 cases (median 25 years, range 0.1–86 years). These were plotted in a separate t-SNE, and the TYA cohort was then plotted with them, to observe more clearly the clustering of the different HGG subgroups in the TYA population.

DNA copy number

DNA copy number was recovered from combined intensities using the conumee package (v1.36.0). This was derived from combined $\log_2$ intensity data based upon an internal median processed using the R packages minfi and conumee to call copy number in 15,431 bins across the genome. Samples were arranged in columns clustered by contiguous categorical copy number states based upon log ratio thresholds of ±0.1 for gain/loss and ±0.5 for amplification and deletion and organized by their DNA methylation subgroups. Clustering used Euclidean distance and a Ward algorithm.

Fusion panel

RNA was successfully extracted from 128 samples. Library preparation was completed using FUSIONPlex Pan Solid Tumor v2 panel (Archer) following the manufacturer's instructions. Libraries were pooled and sequenced aiming to target 2.5 mol/L reads per sample. Analysis was performed using Archer Analysis Unlimited (software v7.1).

DNA sequencing

WES was performed for 107 cases using Agilent SureSelect whole exome v8 at the Institute of Cancer Research core genomics facility. Libraries were pooled and sequenced appropriately aiming for 300× depth. Matched germline DNA was available for 27 samples, which were prepared as above and sequenced at 100x depth. Exome capture reads were aligned to the hg19 build of the human genome using Burrows–Wheeler Aligner v0.7.12 (bio-bwa.sourceforge.net), and PCR duplicates were removed with PicardTools 1.94 (pcard.sourceforge.net). Single-nucleotide variants were called using the Genome Analysis Tool Kit v3.4–46 based upon current best practices using local realignment around indels, downsampling, and base recalibration with variants called by the Unified Genotyper (broadinstitute.org/gatk/). Variants were annotated using the Ensembl Variant Effect Predictor v74 (ensembl.org/info/docs/variation/vep) incorporating SIFT (sift.jcvi.org) and PolyPhen (genetics.bwh.harvard.edu/pph2) predictions, COSMIC v64 (sanger.ac.uk/genetics/CGP/cosmic/), dbSNP build 137 (ncbi.nlm.nih.gov/sites/SNP), ExAc, and ANNOVAR annotations.

Neuropathology assessment

The original slides were centrally reviewed, blinded to the molecular profile. Tumors were reviewed with reference to microscopic criteria reported in the WHO Classification of Tumors of the Central Nervous System, Fifth Edition 2021, including the degree of cellularity, atypia, presence of mitoses, microvascular proliferation, and necrosis (10). Differences in cytologic or architectural appearances were noted and subsequently reviewed in the context of molecular profile.

Statistical analysis

Statistical analysis was carried out using R 4.3.2 (www.r-project.org) and GraphPad Prism 9. Categorical comparisons of counts were carried out using the Fisher exact test; comparisons between groups of continuous variables used the Student t test or ANOVA. Univariate and multivariate differences in survival were analyzed by Cox regression to determine the HRs and significance. All tests were two-sided, and a P value of less than 0.05 was considered significant after multiple testing correction (FDR).

Data availability

All newly generated data have been deposited in the European Genome–phenome Archive (www.ebi.ac.uk/ega) with accession number EGAS50000000641 (sequencing) or ArrayExpress (www.ebi.ac.uk/arrayexpress/) with accession numbers E-MTAB-13974 and E-MTAB-13975 (methylation arrays). Curated gene-level copy number and mutation data are provided as part of the pediatric-specific implementation of the cBioPortal genomic data visualization portal (pedcbioportal.org). The summary data can also be accessed via Synapse (accession number syn64620613; https://www.synapse.org/Synapse:syn64620613). Raw data from this study are available upon request to the corresponding author.

Results

The TYA HGG cohort

Two-hundred and seven of the collected samples, from patients aged 13 to 30 years at diagnosis and from any location within the CNS, underwent DNA methylation profiling, of which 107 cases also underwent WES, and were confirmed to be *IDH* and histone WT HGG (**Fig. 1A**). Tumor location was available for 189 cases; 84.7% ($n = 160$) were hemispheric, and 15.3% ($n = 29$) were identified in a midline anatomical location (**Fig. 1B**). 44.4% ($n = 92$) of the collected cohort were female, and 55.6% ($n = 115$) were male (Supplementary Fig. S1A). The median age was 17.0 years (range 13–30 years). Where the histologic diagnosis was available, 83.7% ($n = 154/184$) were diagnosed histologically as a glioblastoma or HGG; rare cases formerly known as PNET and anaplastic PXA were included due to no available molecular confirmation of these diagnoses. Review of the histology (where available) showed high cellularity, microvascular proliferation, necrosis, and increased mitotic activity. 7.6% ($n = 14$) were diagnosed as a form of anaplastic

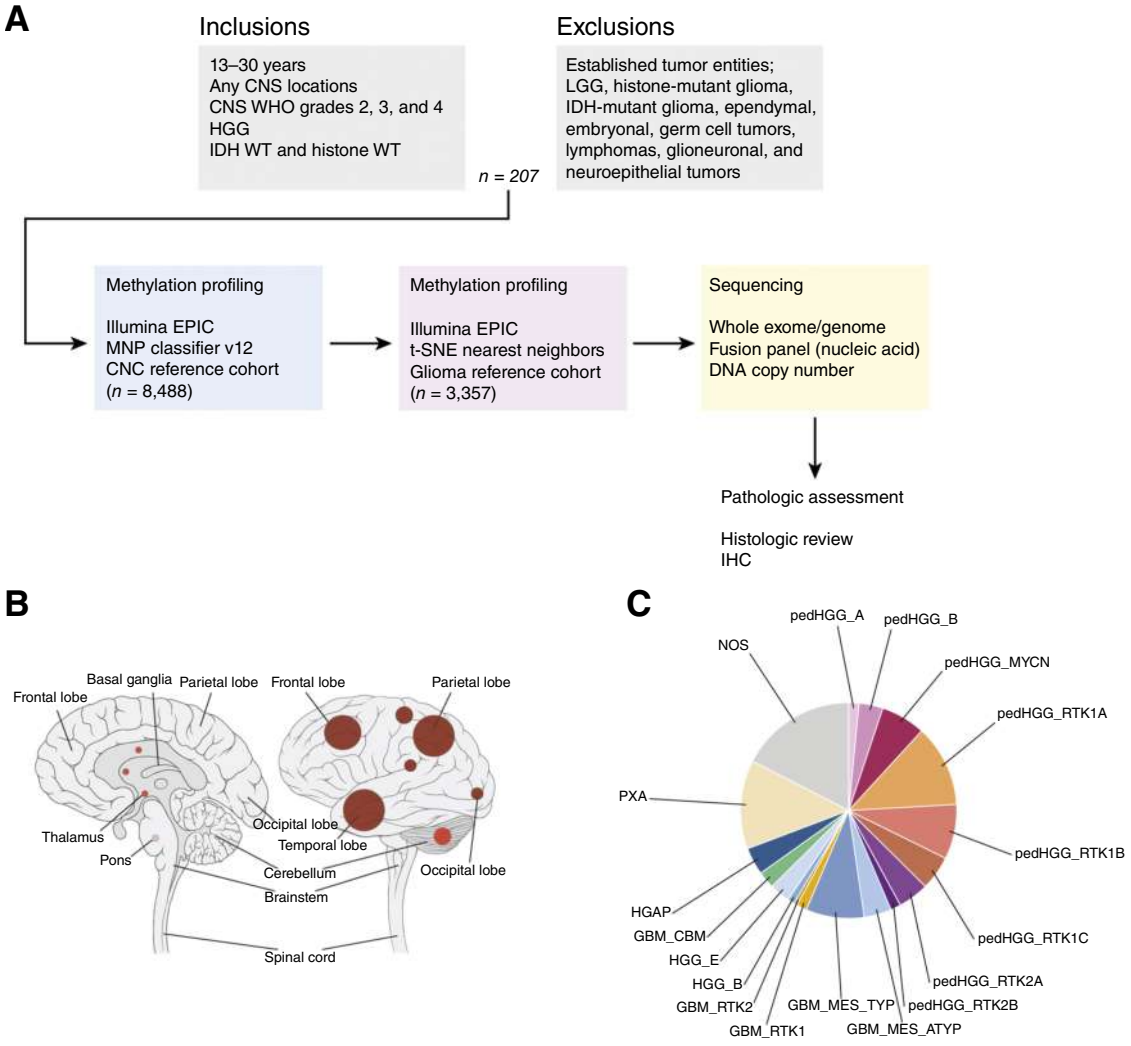

Figure 1.

Defining an intrinsic set of TYA HGGs. **A,** Flow diagram providing an overview of the inclusion and exclusion criteria for the assembled cohort of 207 samples from patients aged >13 to ≤30 years. **B,** Anatomic location of TYA HGG after exclusion of non-glioma entities by methylation profiling ($n = 189$). Left, sagittal section showing internal structures; right, external view highlighting cerebral lobes. Each circle represents the proportion of cases occurring in this location and is colored by the generic locations for hemispheric (brown), midline (red), and brainstem (pink). **C,** Pie chart showing the proportion of different methylation subclasses within the cohort before exclusion of non-glioma entities ($n = 195$). Each subgroup is represented by a different color, as indicated by the key. Cases that scored <0.5 using the MNP classifier v12.8 were classed as "NOS." Twelve cases were excluded based on poor scoring QC parameters of the methylation data.

glioma (a term no longer recognized by the WHO classification in the context of glioma subtypes) (Supplementary Fig. S1B).

Outputs from DNA methylation profiling were used to filter cases with poor QC and those classified as "NOS" (not otherwise specified) due to calibrated scores lower than 0.5. A pan-CNS reference cohort, consisting of 8,488 cases from existing publicly available datasets (2, 8, 16, 21, 24, 25), was constructed and plotted using t-SNE projections (Supplementary Fig. S2A).

Twelve cases did not meet the methylation data QC requirements and so were not included in the methylation data analysis but remained in the cohort and were processed as per other elements of the study. Thirty-seven cases were assigned "NOS," requiring further characterization using alternative integrated diagnostic approaches (**Fig. 1C**). The NOS group did not form distinct methylation clusters using t-SNE, suggesting they did not represent a novel subgroup(s). The remaining 158 cases (excluding NOS cases) were projected onto a reference set of gliomas comprising several HGG entities ($n = 3357$; **Fig. 2A**; Supplementary Table S1). Twenty-nine cases (18.0%) were classified as subgroups more frequently seen in older adults (by current classifier definitions), including GBM_MES ($n = 25$, 15.5%) and GBM_RTK1/2 ($n = 4$, 2.5%). 15.5% ($n = 25$) cases were classified as PXA and 5.0% ($n = 8$) as HGAP, a new entity in the WHO classification.

Clinical treatment information was available for nine cases classifying as PXA. Seven of nine PXA cases achieved a GTR, a single tumor was debulked, and one received a biopsy only. All 9 cases were treated with chemotherapy (reported to be temozolomide in 5 cases) and radiotherapy, and two cases were treated with

radiotherapy alone. Two cases were treated with trametinib and dabrafenib. A combination of dabrafenib and vemurafenib was used for two cases diagnosed as "anaplastic PXA." Survival data comparing PXA with HGAP showed a similar overall survival profile (median OS 28 months vs. 34 months, respectively, $P = 0.5393$ ns; Supplementary Fig. S2B).

Overall, this demonstrated that a relatively small proportion of TYA *IDH* and H3 WT HGGs represent tumor types associated with the adult population.

Pediatric-specific and novel methylation subgroups

When reviewing the classifier assignments and tSNE distribution of the 158 cases (excluding NOS cases), 86 (54.4%) classified as pediatric-type subgroups (by current classifier definitions), including pedHGG-RTK1A/B/C [$n = 51$, 32.3% (47.1% $n = 24$ RTK1A, 31.4% $n = 16$ RTK1B, and 21.6% $n = 11$ RTK1C)], pedHGG-*MYCN* ($n = 13$, 8.2%), and pedHGG-RTK2A/B [$n = 12$, 7.6% (75.0% $n = 9$ pedHGG_RTK2A and 25.0% $n = 3$ pedHGG_RTK2B]. Twenty-three cases were assigned to novel, recently identified, poorly characterized subgroups with distinct methylation profiles, including adult-type diffuse HGG, IDH WT, subtype B (HGG_B, $n = 2$, 1.3%), adult-type diffuse HGG, IDH WT, subtype E (HGG_E, $n = 6$, 3.8%), glioblastoma, IDH WT, subtype posterior fossa (GBM-CBM, $n = 5$, 3.2%), and pedHGG-A/B ($n = 10$, 6.3%; **Fig. 2A**).

The 158 cases were then plotted in a t-SNE alone (**Fig. 2B**). They maintained the expected pattern of clustering according to their methylation profiles, including clustering of those subgroups associated with pediatric populations (e.g., pedHGG_A/B/RTK/*MYCN*, etc.) and adult population (GBM_MES_TYP/ATYP). Similar patterns of clustering to that seen in the glioma reference t-SNE were observed, helping to validate the assignments. This was also confirmed using unsupervised clustering; the pedHGG_RTK tumors clustered together, as did the MAPK pathway–driven tumors (PXA and HGAP cases). Interestingly, the HGG_E cohort formed a distinct cluster with a hypomethylated profile (Supplementary Fig. S2C).

The majority of TYA HGG *IDH* and H3 WT HGGs therefore classify as either a pediatric-type or a poorly understood novel methylation class.

Incidence of tumor subtypes in the TYA age group

To explore the relationship between age and frequency across the different HGG groups and subgroups, we investigated publicly available methylation datasets in combination with our data ($n = 8488$) to create age–density plots for each methylation-defined subgroup of HGG (**Fig. 2C**).

PedHGG_RTK1B ($n = 37$, median age 16.6 years, age–density peak 13.1 years), and pedHGG_B ($n = 23$, median age 31.4 years, age–density peak 16.2 years) show a large proportion of their frequency ($n = 27/38$ and $n = 11/23$, respectively) within the TYA age spectrum of 13 to 30 years. pedHGG_RTK1A ($n = 124$, median 16.6 years, age–density peak 13.1 years) and pedHGG_RTK1C ($n = 53$, median 22.4 years, age–density peak 13.9 years) also frequently occurred within the TYA age group ($n = 54/124$ and $n = 24/53$, respectively). Of those cases classifying as pedHGG_RTK1, seven cases underwent GTR, three debulking procedures, two subtotal resections, and a single case of biopsy only. Fifteen cases were treated with adjuvant chemotherapy (most frequently temozolomide), and 14 were treated with combined radiotherapy. Two patients were treated with chemotherapy or radiotherapy alone. Single cases were treated with a peptide vaccine, bevacizumab, and palliative immunotherapy (nivolumab).

Glioblastoma, RTK1 ($n = 213$, median age 59.4 years, age–density peak 61.4 years), RTK2 ($n = 350$, median age 58.4 years, age density peak 54.2 years), and MES_TYP ($n = 311$, median age 54.5 years, age–density peak 61.6 years) subtypes show an age distribution of patients aged >50 years. GBM_MES_ATYP ($n = 40$, median age 32.7 years, age–density peak 15.0 years), distinct from the GBM_MES_TYP group, shows that 38% ($n = 15/40$) of cases fall within the TYA age group. The pedHGG_RTK1 subgroups also showed a similar distribution, with a higher incidence in the TYA age group compared with the pediatric age group ($n = 105/215$ vs. $n = 86/215$ pedHGG_RTK1), but they are not exclusive to this age. No subgroups show all of their distribution within the TYA age group. With consideration to the number of cases in each subgroup cohort, many of the curves showed a tail characterized by smaller peaks of density occurring outside their peak distribution, and in some subgroups their expected range (e.g., pediatric-type tumors occurring in older adults and adult-specific tumors occurring in the pediatric setting). pedHGG_RTK2A tumors ($n = 58$, median age 13.3 years, age–density peak 12.7 years) showed a greater proportion of cases in the TYA age group than pedHGG_RTK2B tumors ($n = 41$, median age 19.7 years, age–density peak 9.1 years), with $n = 25/58$ and $n = 9/41$, respectively. Clinical annotations for cases classifying as pedHGG_RTK2 indicated one case had a subtotal resection and two underwent biopsy only. Three were treated with both chemotherapy and radiotherapy, one of which was craniospinal due to the identification of metastatic spinal lesions. Chemotherapy consisted of adjuvant temozolomide and second-line procarbazine and lomustine. Re-irradiation was reported in a single case. Survival data for the pediatric-type HGG subgroups showed similar survival profiles (median OS for pedHGG_MYCN 13.0 months, pedHGG_RTK1C 23.0 months, pedHGG_RTK2A 14.7 months, pedHGG_A 14.0 months, and pedHGG_B 20.1 months; Supplementary Fig. S2D).

For the poorly characterized methylation subgroups, HGG_E cases show a broad range of incidence, with a peak at approximately 9.4 years but a median age of 15.8 years ($n = 23$, range 2–64 years), with cases identified across pediatric, adolescent, and young adult ages but declining to very low incidences after age 30 (**Fig. 2C**). HGG_B cases ($n = 8$, median age 35.1 years, age density peak 29.1 years) showed a higher frequency of cases in the TYA age group, though the numbers are small ($n = 6/7$). According to the current classifier definition of the HGG_B and HGG_E groups, they were both "adult-type" diffuse HGG, but such a definition was not reflected by either of the density profiles. The GBM_CBM group ($n = 26$, median age 26.8 years) showed $n = 13/26$ cases occurring in the TYA age group, with a peak at 15.6 years and a range of 2 to 74 years. The pedHGG_B subgroup mimics the trend seen with the GBM_CBM group. The pedHGG_A group ($n = 25$) has a median age of 13.8 years, and the incidence then declines after age 30 years, with a range of 1.3 to 57 years. Clinical annotations for novel entities showed that three cases achieved GTR, and single incidences were observed for STR, tumor debulking, and biopsy alone. One case of GBM_CBM was treated with adjuvant radiotherapy in addition to bevacizumab and was alive at the time of manuscript writing. 4/5 HGG_E cases were treated with adjuvant chemotherapy (temozolomide) and radiotherapy, with the remaining case treated with chemotherapy alone.

When comparing with other molecularly defined HGG subtypes, infant-type hemispheric gliomas ($n = 66$, median age 2.3, age–density peak 0.5 years) characteristically occur in the infant

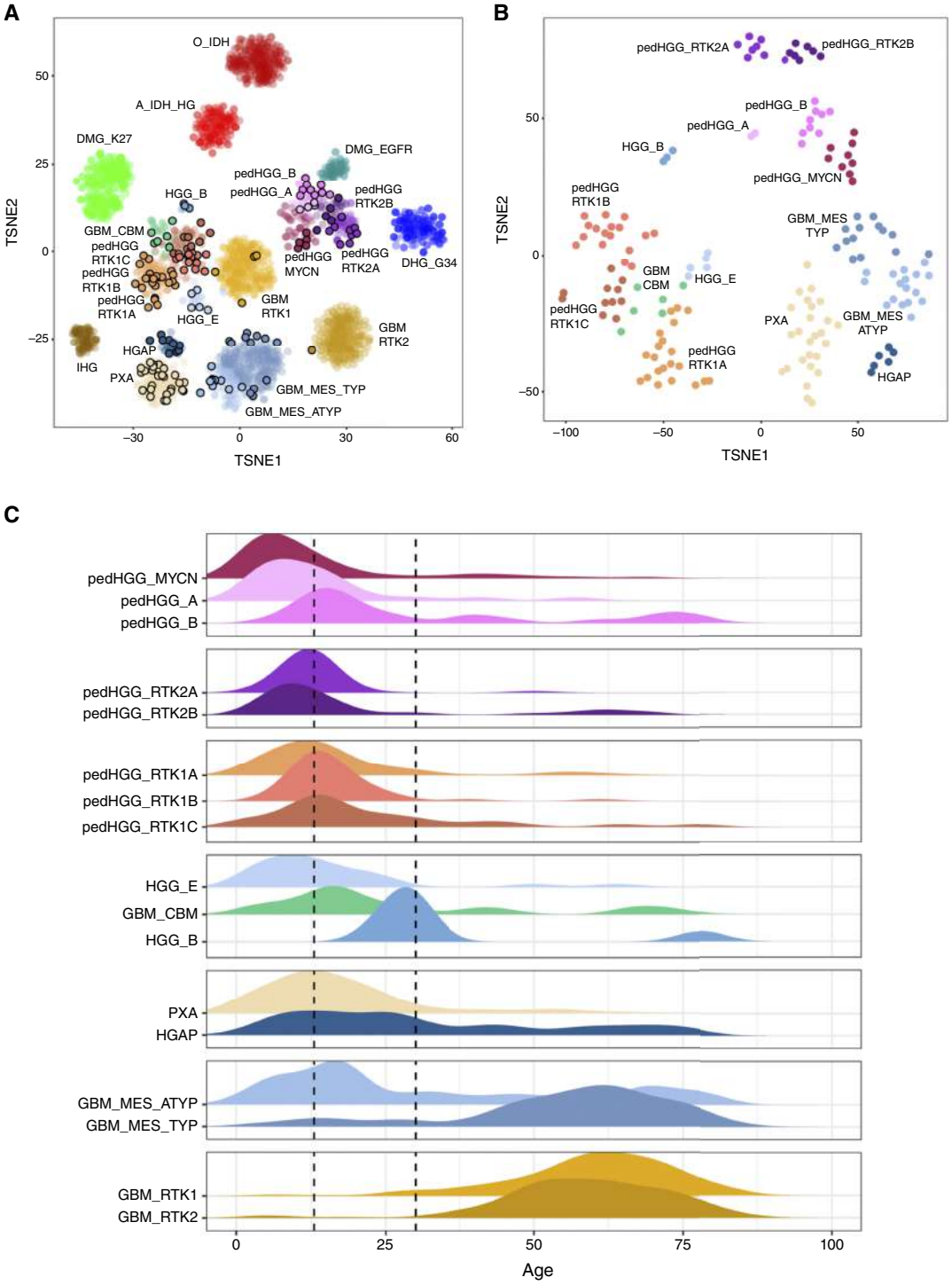

Figure 2.

DNA methylation array profiling of the TYA HGG cohort. **A,** Methylation array profiling and analysis by the Heidelberg classifier excluded 12 cases that failed QC and identified 34 with a calibrated score of <0.5 that were assigned as NOS. t-SNE projection of the remaining 158 cases highlighted cohorts that clustered with both adult and pediatric-type HGG subgroups, including some novel methylation-defined subgroups. Cases then underwent further histopathologic assessment and in-depth sequencing to either confirm the methylation assignment or to further characterize the different subgroups. **B,** t-SNE projection of the collected cohort of 158 TYA cases alone, without the glioma reference set cases. Samples are represented by dots colored by subtype. **C,** Age–density plot showing the age distribution and peak incidences of different HGG subtypes by DNA methylation profiling, comprising 1,704 cases derived from the collected TYA cohort and published datasets. Tumors are grouped according to methylation subclasses and predicted age distribution according to the WHO classification. Dotted lines define the age cut-off for the TYA group in this project (13 and 30 years).

population, whereas the diffuse hemispheric glioma, G34-mutant (DHG_G34; $n = 181$, median age 19.1 years, age–density peak 14.3 years), IDH-mutant high-grade astrocytomas (A_IDH_HG; $n = 221$, median age 35.6 years, age–density peak 32.9 years), and diffuse midline glioma, H3 K27-altered (DMG_K27; $n = 357$, median age 11.4 years, age–density peak 6.5 years) show a proportion of their frequency within the TYA age spectrum of 13 to 30 years (Supplementary Fig. S2E).

Therefore, no methylation subclasses of HGG are exclusive to the TYA age group, although some show a peak in their distribution in the 13 to 30 year range (including HGG_B, GBM_CBM, and GBM_MES_ATYP), and more generally, pediatric- and adult-type HGG groups show a wider age distribution than perhaps would be expected.

Copy number profiling

Copy number data derived from the Illumina array were available for all 207 cases. Review of the clinical annotations associated with the glioma reference cohort identified that 8310/11933 (69.6%) cases were annotated for age, and of these, 276 cases correlated with the study inclusion criteria and were within the TYA age range. After excluding cases classified as NOS or failing to meet the methylation QC parameters, 158 cases were combined with those derived from the glioma reference cohort (giving a total of $n = 434$) and were clustered within their respective methylation subgroups (**Fig. 3A**). Subtype-enriched profiles were observed, including the classical gain of chr7 and loss of chr10 seen in the GBM_MES_TYP and GBM_RTK1 subgroups, consistent with the pattern of adult HGG. The methylation-defined pediatric-specific subgroups showed more variable profiles with changes frequently involving chr1. The pedHGG_*MYCN* tumors were enriched for gains of chr1, 2, and 7.

When the same cohort was clustered by copy number change across the methylation subgroups, frequent changes across the cohort included chromosomal gains [chr1q (54%), chr2 (22%), and chr7 (41%)] and losses [chr10 (40%) and chr13 (64%; Supplementary Fig. S3].

Focal amplifications seen in the cohort included *PDGFRA* (5.8%), *CDK4* (3.9%), *MYCN/ID2* (4.3%), *MYC* (1.4%), *CDK6* (1.4%), and *EGFR* (1.0%), and the most common focal deletion was *CDKN2A/p16* (19.2%). Across the combined cohort of 434 cases, similar patterns were seen,as well as amplifications in *KIT* ($n = 14$, most frequent in the pedHGG_RTK1B subgroup), *MET* amplifications [$n = 4$, seen in pedHGG_RTK1C ($n = 2$), HGG_B ($n = 1$), and PXA ($n = 1$) subgroups] and a higher frequency of *EGFR* amplifications [$n = 15$, seen across GBM_RTK2 ($n = 4$), pedHGG_*MYCN* ($n = 4$), pedHGG_RTK2A ($n = 4$), and pedHGG_A ($n = 3$) subgroups)] were identified (**Fig. 3B** and **C**; Supplementary Tables S2 and S3).

TYA HGGs therefore show the characteristic copy number changes and gene amplifications and deletions, which are known to

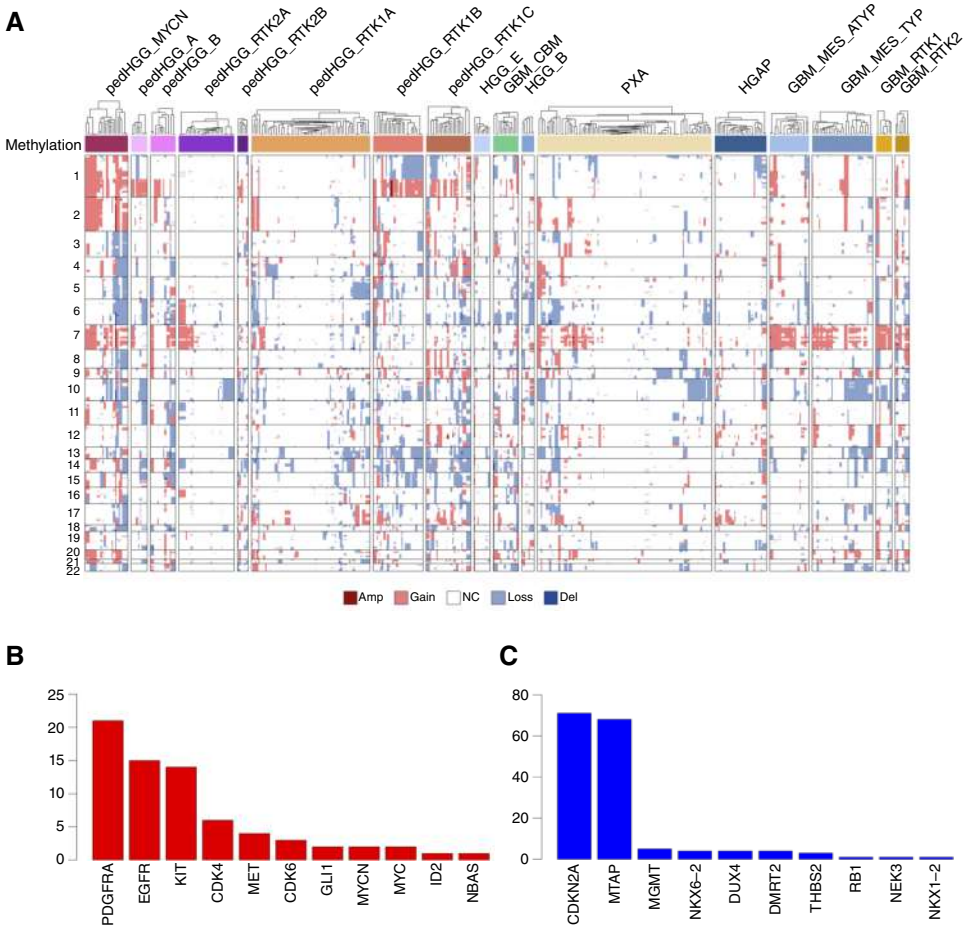

Figure 3.
DNA copy number profiling of TYA HGG. **A,** Heatmap representation of segmented DNA copy number for 434 cases of TYA glioma profiled on the Illumina 450k or EPIC BeadArray platform (dark red, amplification; red, gain; dark blue, deletion; and blue, loss). Samples are arranged in columns clustered by contiguous categorical copy number states based upon log ratio thresholds of ±0.1 for gain/loss and ±0.5 for amplification and deletion and organized by their DNA methylation subgroups. Clustering used Euclidean distance and a Ward algorithm. Methylation annotations are provided as a bar according to the included key. **B,** Frequency bar plot showing the most frequent amplifications identified from the copy number profiles across the cohort ($n = 434$). **C,** Frequency bar plot showing the most frequent deletions identified from copy number profiles across the cohort ($n = 434$). Amp, amplification; Del, deletion. NC, no change.

occur across the HGG spectrum but are enriched in specific methylation subclasses.

Somatic mutational landscape of TYA HGG subgroups

WES data were available in 107/207 cases (**Fig. 4**; Supplementary Table S4). Of the cases, 27 were assigned as NOS (calibrated score <0.5), and 12 cases whose methylation data were excluded due to inadequate QC parameters also underwent WES. Cases were grouped according to their HGG subgroup based on their DNA methylation profiles; some of the variants detected (and the pattern of incidence) from the NOS and methylation QC-failed group paralleled the known methylation profiles. The essential and desirable diagnostic criteria from the current WHO classification (12) were applied when grouping these cases accordingly. If the methylation or variant profiles could not support a reliable assignment, they were grouped according to the variant type seen, e.g., MAPK pathway–altered ($n = 8$), *MYCN*-amplified ($n = 2$), and *CDKN2A/B/p16*-deleted ($n = 6$).

Pathognomonic mutations of tumor subgroups were detected, including the presence of *CDKN2A/B* alterations and MAPK pathway alterations (e.g., *BRAF* V600E mutations) in PXA ($n = 9$) and *CDKN2A/B* alterations and *ATRX* mutations in HGAP ($n = 3$). The most frequent glioma-associated variants included *TP53* ($n = 65$), *NF1* ($n = 35$), *PDGFRA* ($n = 28$), and *EGFR* ($n = 18$; Supplementary Fig. S4A).

Eight cases from the cohort showed a hypermutator phenotype (mutation frequency ranging from 2,817 to 5,273) with frequent mutations in *TP53, ATRX, PDGFRA, BCOR, SEDT2, NF1,* and *RB1* (**Fig. 4**). Three of these cases classified as the novel HGG_E methylation subgroup, suggesting a somatic mutational signature of this group. Others included pedHGG_RTK1 ($n = 1$) and GBM_CBM ($n = 1$) cases and also tumors which did not classify as any of the currently recognized entities ($n = 3$, NOS).

Current adult defined subtypes, including GBM_MES ($n = 15$) and GBM_RTK1 ($n = 3$), were enriched for the presence of *PTEN* variants ($n = 8/18$) and *CDK4* amplifications ($n = 2/3$ in GBM_RTK1) in addition to frequent variants in *TP53* ($n = 12/18$).

The current pediatric subtypes also showed distinct signatures compared with other subgroups of HGG; as expected, the pedHGG_RTK1A/B/C subgroups were all enriched for *PDGFRA* alterations (mostly amplifications; $n = 11/16$) as well as *TP53* ($n = 11/16$) and *ATRX* ($n = 6/16$) variants and variable incidences of *CDKN2A/B*, *BCOR*, *SETD2*, and *NF1* alterations (**Fig. 4**). Nine cases were assigned to a "pedRTK1-like" group based on *PDGFRA* ($n = 8$) alteration. The pedHGG_*MYCN* subgroup was associated with *MYCN* amplifications, although this was not a universal feature of high-scoring tumors in the *MYCN* subgroup ($n = 3/7$). Two further NOS/methylation QC-failed cases contained a *MYCN* amplification and, in the absence of other subgroup-identifiable features, were assigned to a *MYCN*-like group.

Three cases classifying as the novel GBM_CBM group showed a variable incidence of variants, including the hypermutator

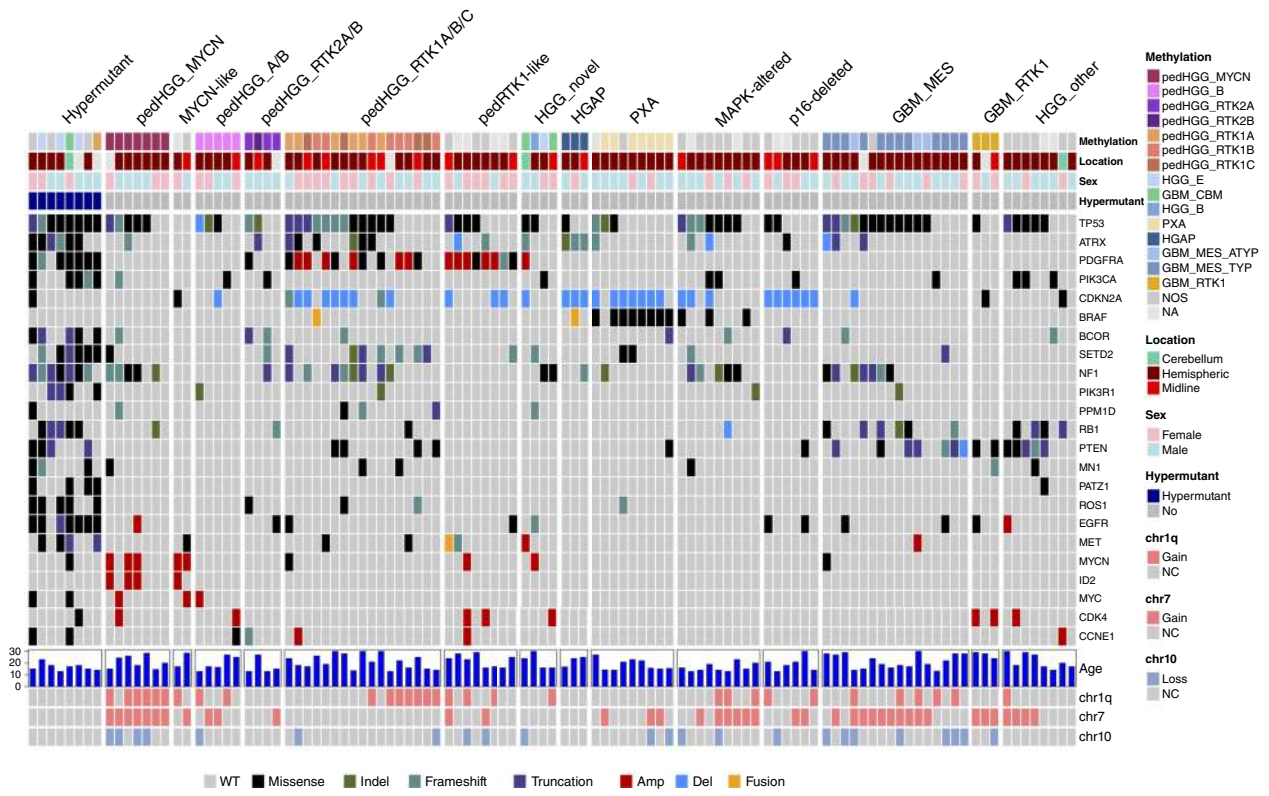

Figure 4.

Mutations in TYA gliomas. OncoPrint representation of an integrated annotation of single-nucleotide variants, DNA copy-number changes, and structural variants for TYA gliomas ($n = 107$). Samples are arranged in columns with genes labeled along rows and are grouped by methylation subclass and landscape of variants. Clinicopathologic and molecular annotations are provided as bars according to the included key. Amp, amplification; Del, deletion; NA, not available; NC, no change.

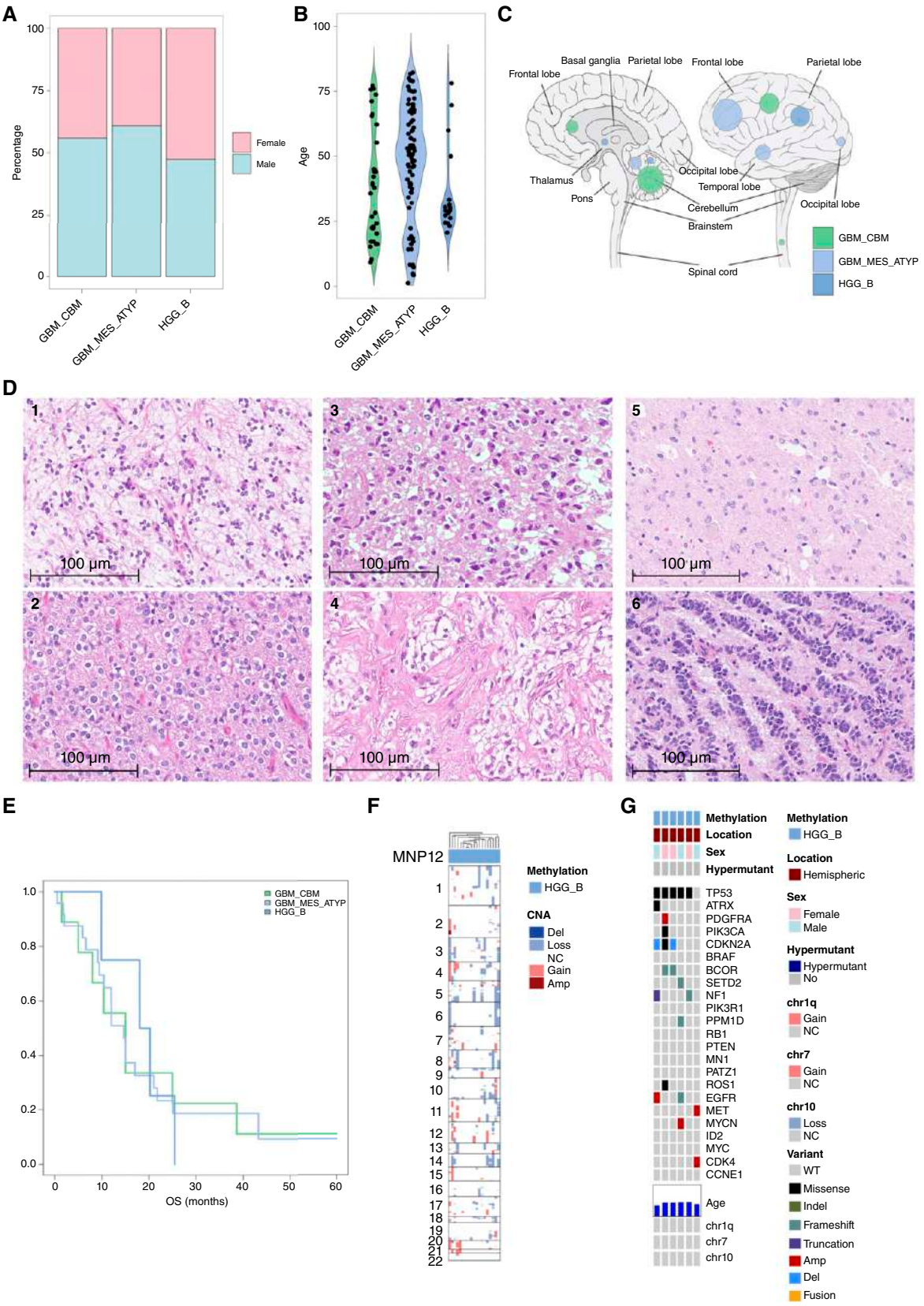

phenotype in one case, *ATRX* and *PDGFRA* variants, and nonspecific range of variants in genes frequently mutated in HGG, including *BCOR*, *SETD2*, *NF1*, *RB1*, and *CDK4* amplifications.

Eight cases contained variants frequently seen in HGG, but the profile of these and the available neuropathologic or molecular data did not support a reliable assignment, and they were therefore grouped as "HGG_other" (**Fig. 4**).

ArcherDX fusion panel sequencing was performed on 92/207 (44.4%) cases (Supplementary Fig. S4B) and identified isolated examples of RTK fusions (*PRPTZ1::MET* and *GOPC::ROS1* fusions). These alterations were validated by indicative small copy number changes, showing that RTK fusions are not a frequent feature in TYA HGGs. A single *KIAA1549::BRAF* fusion was identified in an HGAP case, which is a recognized molecular feature in a subset of these tumors.

TYA HGGs therefore show mutational landscapes which may be targetable, and an integrated diagnostic approach can be used to assign cases to methylation- or variant-based cohorts to help guide management.

Characteristics of poorly described methylation-defined subgroups and clinical correlations

This study has identified three HGG subgroups occurring more frequently in TYAs, including GBM_CBM, HGG_B and GBM_MES_ATYP, all of which were considered poorly described methylation subgroups. We gathered all publicly available data, and from a local adult-based diagnostic center, for these rare groups, irrespective of age, to review their characteristic features [HGG_B ($n = 19$), GBM_CBM ($n = 34$), and GBM_MES_ATYP ($n = 102$)]. The GBM_MES_ATYP subgroup occurred more frequently in males ($n = 62/102$; **Fig. 5A**). The median age for GBM_CBM was 36.8 (range 9–77 years), GBM_MES_ATYP was 50.4 (range 1–82 years), and HGG_B was 29 (range 23–78 years; **Fig. 5B**). There is a peak of distribution in the TYA age group for GBM_CBM and GBM_MES_ATYP. However, for the GBM_CBM subgroup, there is a long tail of distribution extending into older adults, and for the GBM_MES_ATYP, a large, broad peak in older patients. The HGG_B subgroup, however, is a TYA-specific subgroup. Although the current naming of the GBM_CBM group implies they occur in the cerebellum, this is not always the case, with 4/27 cases (14.8%) with available location information reported in a hemispheric location (either frontal or temporal lobes) and single cases in the thalamus and spinal cord (**Fig. 5C**).

Histology showed features consistent with a HGG, including the presence of multinucleated giant cells for all subtypes (**Fig. 5D**; Supplementary Fig. S5A). The TYA-specific HGG_B subgroup showed heterogeneous appearances. Some tumors showed perinuclear clearing [**Fig. 5D**(1–4)] with round to oval atypical nuclei. However, they also showed variable architectural features; rare cases showed a nested architecture surrounded by a more fibrous-like stroma [**Fig. 5D**(4)], and others showed a low to moderate cellularity with a more infiltrative pattern [**Fig. 5D**(5)]. A single case showed focal areas with an embryonal-like appearance comprising hyperchromatic and pleomorphic irregular shaped nuclei which showed a distinct palisading architectural pattern [**Fig. 5D**(6)]. Three of nine cases showed the presence of microcalcifications. GBM_CBM histology showed a highly cellular and infiltrative glial tumor, with a subset of cases showing perinuclear clearing, set within a fibrillary stroma (Supplementary Fig. S5A1–5). The nuclei were round to oval, with variable degrees of nuclear pleomorphism (Supplementary Fig. S5A5). Some cases showed oval-shaped or spindled nuclei, and others contained cells with a "pennies on a plate" or multinucleated morphology (Supplementary Fig. S5A1–5). Small, thin-walled branching vessels were interspersed within the tumors. GBM_MES_ATYP cases comprised a highly cellular glial tumor set within a fibrillary stroma. The tumor cells formed a dense sheet-like architecture. The nuclei showed variable degrees of atypia (including very markedly atypical and large nuclei) and frequently displayed pale chromatin with prominent nucleoli, surrounded by pink eosinophilic pale, granular, or glassy cytoplasm (Supplementary Fig. S5A6–10). Multinucleated cells were also common (Supplementary Fig. 5A6–8). Rare cases showed focal collections of more primitive-appearing cells (Supplementary Fig. S5A9), and cases frequently showed distinct areas of inflammatory cell infiltrates (12/39 cases; Supplementary Fig. S5A10). Limited available survival data show that the HGG_B, GBM_CBM, and GBM_MES_ATYP groups have a poor prognosis (median OS 19.1, 22.6, and 7 months, respectively; **Fig. 5E**).

Copy number profiling data for HGG_B ($n = 19$) showed considerable variability with no distinctive patterns (**Fig. 5F**). GBM_CBM ($n = 34$) also showed considerable variability with no distinctive differences between patients aged <30 or >30 years (Supplementary Fig. S5B). The GBM_MES_ATYP cases ($n = 102$) showed frequent gains of chr7 associated with chr10 loss (18.6%, $n = 19/102$) compared with GBM_MES_TYP (15.2%, $n = 5/33$, $P = 0.7960$) but also a proportion of cases which contained just chr7 gains (19.6%, $n = 20/102$), lower than the proportion with this change seen in GBM_MES_TYP (27.3%, $n = 9/33$; $P = 0.3421$). When looking at cases of GBM_MES_ATYP aged <30, these cases were more frequently associated with a gain of chr7 alone (36.8%, $n = 7/19$) compared with those aged >30 (15.6%, $n = 13/83$; $P = 0.0528$), and a subset of these were also associated with a gain of chr1 (21.1%, $n = 4/19$), and a proportion of cases containing gains of chr6 (21.1%, 4/19). There was a higher frequency of cases which contained neither change in the GBM_MES_ATYP group (40.2%, $n = 41/102$) compared with GBM_MES_TYP (30.3%, $n = 10/33$; $P = 0.4092$; Supplementary Fig. S5B). Sequencing data show *TP53* variants ($n = 5/6$) and amplifications, including *MYCN* ($n = 1/6$), *EGFR* (2/6), *MET* (1/6), *CDK4* (1/6), and *PDGFRA* (1/6), in the

Figure 5.

Characterization of a true TYA HGG subgroup using the collected cohort and publicly available cases with DNA methylation profiling data. **A,** Gender bar plots showing the gender distribution of the available cases for GBM_CBM, HGG_B, and GBM_MES_ATYP subgroups. **B,** Violin plots showing the age distribution and median age of the available cases for GBM_CBM, HGG_B, and GBM_MES_ATYP subgroups. **C,** Anatomic location of poorly characterized HGG subgroups irrespective of age. Left, sagittal section showing internal structures; right, external view highlighting cerebral lobes. Each circle represents proportion of cases occurring in this location and is colored by the tumor subgroups. **D,** Representative hematoxylin and eosin images of the HGG_B subgroup. **E,** Kaplan–Meier showing OS available by methylation subclass (line color as per key) for TYA-specific subgroups ($n = 12$). **F,** Heatmap representation of segmented DNA copy number for the HGG_B subgroup (dark red, amplification; red, gain; dark blue, deletion; and blue, loss). Samples are arranged in columns clustered by contiguous categorical copy-number states based upon log ratio thresholds of ±0.1 for gain/loss and ±0.5 for amplification and deletion. Clustering used Euclidean distance and a Ward algorithm. Methylation annotations are provided as a bar according to the included key. **G,** OncoPrint representation of an integrated annotation of single-nucleotide variants, DNA copy-number changes, and structural variants for the HGG_B subgroup. Samples are arranged in columns with genes labeled along rows and are grouped by methylation subclass. Clinicopathologic and molecular annotations are provided as bars according to the included key. Amp, amplification; Del, deletion; NC, no change.

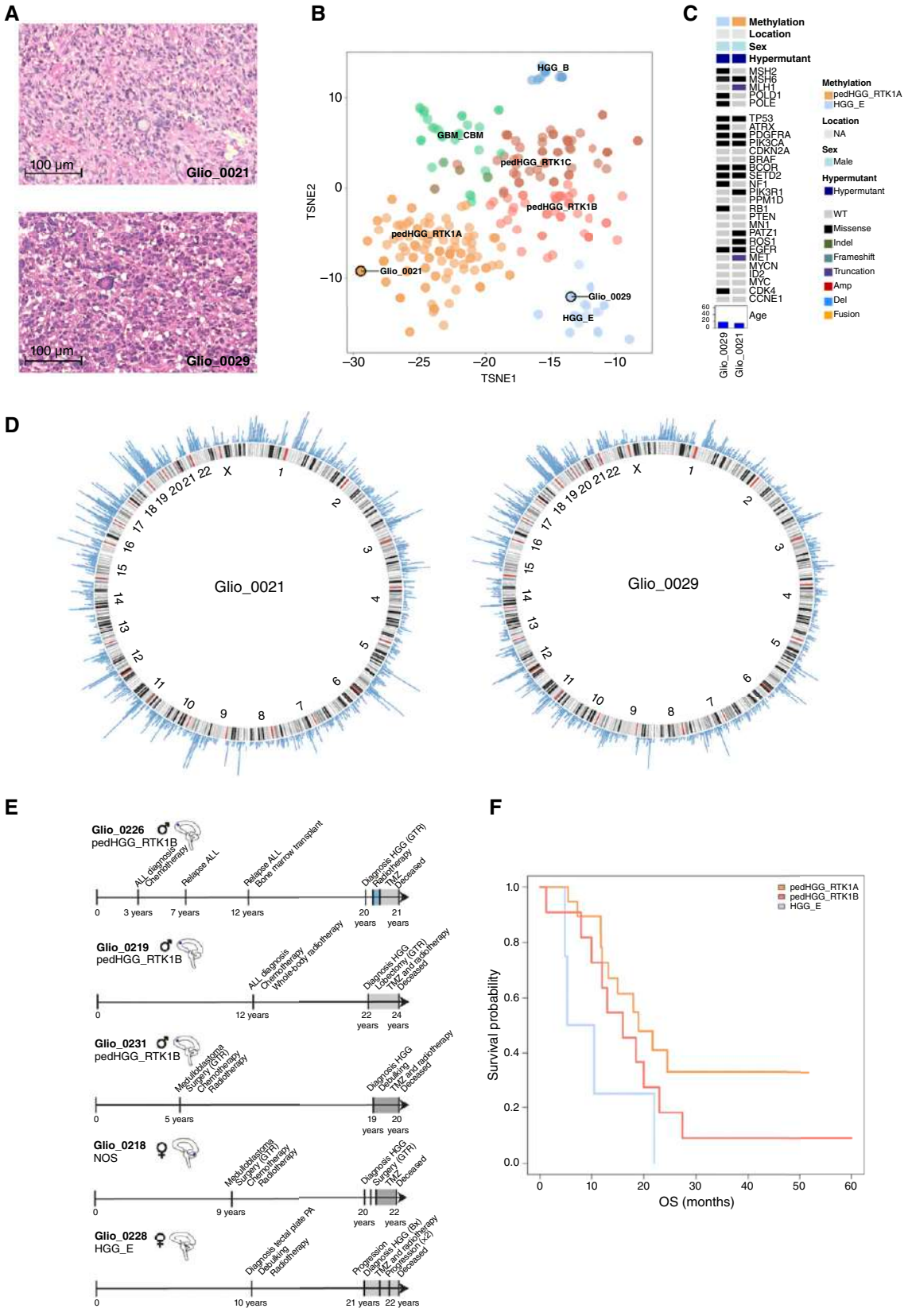

HGG_B cases (**Fig. 5G**). There is enrichment of *CDKN2A/B* deletions in the GBM_CBM group ($n = 7/10$), and *RB1* ($n = 3/13$), *PTEN* ($n = 6/13$), *NF1* ($n = 5/13$), and *TP53* (10/13) alterations occur more frequently in the GBM_MES_ATYP group (Supplementary Fig. S5C). When plotting methylation data of GBM_MES_ATYP cases alone into a tSNE and annotating them by age, no age-defined clustering was seen (Supplementary Fig. S5D).

Clinically, 3/5 GBM_MES cases achieved a GTR with two cases of subtotal resection. Three cases reported treatment with adjuvant chemotherapy and radiotherapy. In addition, one patient received nivolumab, ipilimumab, and regorafenib during the course of their treatment. Re-irradiation was used in a single case. Cases classifying as GBM_MES_TYP showed an improved survival when compared with the GBM_MES_ATYP group (median OS 18 vs. 7 months, $P = 0.05463$; Supplementary Fig 5E).

Several cases associated with tumor predisposition syndromes were identified; interestingly, two patients were siblings (Glio_0021 and Glio_0029). Glio_0021 was reported to have Turcot/mismatch repair syndrome, and Glio_0029 was reported to have constitutional mismatch repair deficiency syndrome (CMMRD). Both tumors showed histologic features of a HGG, with the presence of multinucleated cells (**Fig. 6A**), and were hypermutant but classified differently by methylation profiling (pedHGG_RTK1A and HGG_E, respectively; **Fig. 6B–D**). Glio_0004 was identified to have Li Fraumeni syndrome, and Glio_0272 (HGG classifying as a pedHGG_RTK1A) was found to have biallelic somatic inactivation of *MSH2*, but germline samples were not available.

Of 70 cases, 6 (8.6%) were treated for a previous childhood malignancy before the diagnosis of an HGG (**Fig. 6E**); Glio_0228 was treated for a tectal plate pilocytic astrocytoma (including radiotherapy) but was subsequently diagnosed with an HGG 11 years later, in a similar location, classifying as an HGG_E tumor. Glio_0219 had a history of acute lymphoblastic leukemia (ALL) as a child, treated with chemotherapy and whole-body radiotherapy, and was subsequently diagnosed with an HGG at age 22 which classified as pedHGG_RTK1B. Similarly, Glio_0226 was also treated for ALL as a child with chemotherapy and then diagnosed with a pedHGG_RTK1B tumor at age 20. Glio_0272 was diagnosed with ALL at age 7 months and was initially treated with chemotherapy but underwent radiotherapy treatment at age 5 years when the disease recurred; they were later diagnosed with a pedHGG_RTK1C tumor. Glio_0224 was treated with radiotherapy for ALL at age 2 years and then diagnosed with a tumor classifying as a PXA. An NOS case (0.22 scoring GBM_CBM, Glio_0218) was treated for a desmoplastic medulloblastoma as a child with chemotherapy and radiotherapy and subsequently diagnosed with an HGG at age 20. HGG_E cases showed a worse OS when compared with pedHGG_RTK1A and pedHGG_RTK1B cases in the cohort (median OS survival of 7.9, 16.0, and 16.0 months respectively; **Fig. 6F**).

Multivariate analyses show that the pedHGG_RT1B and HGG_E methylation classes were associated with poor survival [HR 1.69 (0.827–5) $P = 0.15$ and 3.53 (2.26–13.4) $P = 0.041$, respectively; Supplementary Fig. S6A]. The GBM_MES_ATYP methylation subclass also was significantly associated with poor outcomes [3.86 (2.47–14.6) $P = 0.03$]. Mutations in *SETD2* and *MET* were also associated with worse survival compared with WT cases [HRs 2.02 (1.03–6.12) $P = 0.07$ and 2.19 (1.41–8.33) $P = 0.18$, respectively; Supplementary Fig. S6B]. Amplifications in *MET, CDK4, MYCN,* and *PDGFRA* were associated with worse survival, whereas *CDKN2A/B* deletions did not affect survival (Supplementary Fig. S6C). GTR with adjuvant chemotherapy alone was significantly associated with worse outcomes [HR 4.26 (2.92–17.8) $P = 0.03$], as was the decision to undertake a biopsy rather than a resection [HR 2.63 (1.42–8.33) $P = 0.026$; Supplementary Fig. S6D]. *PDGFRA* and *TP53* mutations were significantly associated with a worse OS within the TYA cohort compared with WT cases [HRs 3.36 (1.96–11.4) $P = 0.014$, and 2.07 (0.922–5.8) $P = 0.013$, respectively; Supplementary Fig. S6B, S6E, and S6F]. However, in many cases throughout these analyses, the numbers are small, and therefore these results should be treated with caution.

Discussion

TYA HGGs are a diverse group of tumors, sharing many clinical challenges of HGGs occurring in other age groups. The limited research in this age group, with few studies and limited molecular data currently available, has further affected management (15). The current study investigated a large international multi-institutional cohort of TYA HGGs to provide greater insights into their spectrum. An integrated approach to tumor classification and characterization, using DNA methylation profiling, fusion panel, WES, and histologic review, highlighted the importance of this approach when adopted in diagnosis and tumor stratification (26).

In the United Kingdom and Europe, the age definition of TYAs is 15 to 24 years (ref. 27). The WHO classification recognizes that there are adult-type and pediatric-type HGGs but that these tumors can occur outside of these predicted profiles. The rationale to use the age range of 13 to 30 years was to explore whether there were specific tumor types with a median incidence occurring within the TYA window but also to explore the possible tails of distribution beyond the classic age limit; pedHGG_A (median age 13.8), HGG_E (median age 15.8), pedHGG_RTK1A/1B/1C (median ages 16.6, 16.6, and 22.4, respectively), pedHGG_RTK2B (median age 19.7), and PXA (median age 17.3) all had a median age within the 13 to 30 window. Although the median age for the HGG_B group was 35.1 years, the age–density peak was 29.5 years; the MNP classifier currently defines this as an "adult-type diffuse HGG, IDH WT tumor," but our study highlights that this may not be the case and that it may correlate more closely with other pediatric-type subgroups or be a true TYA subgroup. With the acquisition of additional methylation data for GBM_CBM and GBM_MES_ATYP cases, irrespective of age, their median ages were

Figure 6.

Tumor predisposition syndromes and treatment for childhood malignancies within the TYA cohort. **A,** Hematoxylin and eosin images showing different cytologic and architectural features of the two cases. **B,** t-SNE projection of selected subgroups from the glioma reference cohort. Samples are represented by dots colored by subtype. The sibling cases are highlighted by the black circles and labeled. **C,** OncoPrint representation of an integrated annotation of single-nucleotide variants, DNA copy-number changes, and structural variants for the sibling cases. Samples are arranged in columns with genes labeled along rows. Clinicopathologic and molecular annotations are provided as bars according to the included key. **D,** Circos plots demonstrating the hypermutator phenotypes of the sibling cases. Chromosomal locations are represented by ideograms arranged around the circle. **E,** Patient timelines for five patients identified within the cohort who were treated for a childhood malignancy. Gender is annotated using symbols, and a sagittal brain image demonstrates the location of the tumor. A timeline provides details of key events throughout the course of treatment. **F,** Kaplan–Meier showing OS available for HGG_E, pedHGG_RTK1B, and pedHGG_RTK1A cases, (line color as per key) for the collected cohort ($n = 34$). Amp, amplification; Del, deletion; TMZ, temozolomide.

36.8 and 50.4 years, respectively. However, despite this not being a population-based study, GBM_CBM shows a long tail of distribution extending into older adults, and the GBM_MES_ATYP shows a bimodal distribution, including the TYA window. The age–density plots for different HGG subgroups in this study highlight that age is important but not an arbitrary singular cut-off; it should be more appropriately defined by distribution medians and confidence intervals. Broad age inclusion criteria (or no age exclusions) will be helpful to consider in future studies; HGG subtype–specific studies could focus on identifying cases via their molecular characteristics, rather than an age definition. Comparative studies with other published cohorts will therefore require the prioritization of molecular profiling (including the use of DNA methylation profiling), opposed to comparative age inclusion criteria.

Within this study, we accepted an MNP12 calibrated score of >0.5 as acceptable for classification. The use of scores >0.9 in Capper and colleagues (8) 2018 as well as the MNP website is a conservative threshold. For example, if a calibrated score of >0.9 is not achievable, the classifier can still assign the case to a glioma family group. Also, tumor classification was undertaken by integrating MNP classifier outputs, sequencing data, and clinical information, utilizing the integrated approach used in the neuropathology diagnostic setting. It is also important to consider the context of this study which is an exploratory research project, helping to refine future diagnostic practice. Therefore, the need for diagnostic precision, in which the output will influence treatment in individual cases, is not the goal. A calibrated score of <0.9 should not automatically mean that the class assignment is not of value (9); many factors can influence the score, including the cellularity, tumor percentage, and the presence of necrosis. However, if the assignment is still comparable with the histologic features or other sequencing results (which provide a further level of scrutiny), then this can still support the diagnosis. The copy number data derived from the Illumina array data is also very valuable, illustrating characteristic copy number changes which can either support or refute the suggestion by the classifier or the neuropathologist's suspicions. If genomics data, copy number changes, histologic features, and the t-SNE position align, the inclusion of cases with a score <0.9 was justified.

Rare subgroups showed a peak age distribution in the TYA age group (GBM_CBM, GBM_MES_ATYP, and HGG_B) compared with pediatric (<13) and adult (>30) ages. Distinct patterns of copy number are seen between all three of these subgroups when comparing data from tumors occurring in those aged <30 versus > 30 years, most prominently with the GBM_MES_ATYP group. At this stage, methylation does not seem to suggest that those occurring in patients aged <30 are a different subgroup, but further sequencing data and clinical annotations are needed to explore whether the distinctions in copy number represent a solitary molecular difference.

The GBM_CBM group is currently defined by the methylation classifier as occurring in the cerebellum. Early studies on cerebellar glioblastoma showed that they were seen more frequently in younger patients with a median age of 52 years (range 5–88 years) and classified predominantly as anaplastic astrocytoma with piloid features (now known as HGAP) and the former GBM_MID methylation class, with the tumors demonstrating similar methylation profiles to DMG_K27 tumors, but with an absence of the histone mutation (28). However, there are other methylation subgroups which are found in this location but of lower frequency, including GBM_MES, GBM_RTK1, and GBM_RTK2, leading authors to suggest that they do not represent a molecularly uniform tumor (28). However, our study suggests otherwise, that there is in fact a distinct methylation subgroup, with a peak of distribution in the TYA window and some potentially occurring after radiotherapy or treatment for medulloblastoma in childhood. Interestingly, despite implications of current terminology in the classifier, they do not occur exclusively in the cerebellum.

The HGG_B group seems to be the only true TYA subgroup identified within this study, and there are currently no published studies focused on this subgroup. They can occur in hemispheric, midline, and posterior fossa locations and display a variable copy number profile, with some changes more specific to those patients aged <30. Alongside frequent *TP53* alterations and variable incidences of *CDKN2A/B* deletions, *BCOR* alterations, and amplifications across different genes, including *MYCN*, *MET*, and *CDK4*, seem to be characteristic features. Histologically, they showed variable appearances, but a proportion was noted to be associated with microcalcification. Therefore, DNA methylation profiling remains the crucial molecular test for diagnosis. Larger cohort studies including *in vitro* and *in vivo* work are needed to further explore targetable associations.

Although clinical annotations were incomplete, there is a suggestion of better survival in some pediatric-type subgroups, including pedHGG_RTK1A, but more data are needed to validate this trend. There are several tumor predisposition syndromes associated with HGGs, including CMMRD and Li Fraumeni (29, 30), and this study identified several incidences of these. Tumors which occur as a result of DNA replication repair deficiency contain pathogenic variants in polymerase-proofreading genes and/or mismatch repair genes (31). Existing studies report a median age of 50 years (range 27–78 years), an association with the histologic giant cell variant of GBM, and most frequently classifying as the pedHGG_RTK1A methylation group (32). They contain high mutation and microsatellite burdens, but their association with high T-cell infiltration leads to the optional use of immune checkpoint inhibition; synergistic combinations (the addition of ipilimumab and the use of MEK-inhibition) have shown promise in those cases in which immune checkpoint inhibition does not work (33, 34). In one study, 4/5 cases classifying as pedHGG_RTK1A and treated with immune check point blockage survived greater than 3 years, and there was an OS of 36.8 months compared with 15.5 months for other HGGs in the study (32). Hypermutation can also be induced by temozolomide treatment in both IDH-mutant and IDH WT LGG and HGG (31, 35), which is an important consideration for tumors that may have undergone transformation to a higher-grade glioma and the potential value of longitudinal sampling to monitor molecular changes as treatment progresses. One such case in our cohort of a tectal plate pilocytic astrocytoma which was treated with radiotherapy and years later was diagnosed with an HGG is a case in point. Similarly, we report siblings with CMMRD; novel homozygous *MSH6* mutations have been previously reported in siblings, resulting in an HGG and T-ALL in an 11-year-old female and a GBM in her 10-year-old brother, both of which rapidly progressed (36).

Ionizing radiation is the only known risk factor for the development of a secondary HGG, but the incidence is only at 1% (37, 38), with variable latency periods seen across all age spectrums (39). A striking feature of our cohort was that 8.6% of cases had been treated for a childhood malignancy (most frequently ALL or a medulloblastoma of the cerebellum), with a subsequent HGG diagnosis in their adolescent years. The risk that previous radiation poses for the development of HGGs has been reported in the literature (39–42), and it is important to recognize that these secondary tumors occur in the TYA population, classifying as primarily pedHGG_RTK1B or HGG_E subgroups in our cohort.

Existing studies also show that these tumors cluster with the pedHGG_RTK1 subgroups and are associated with *PDGFRA* and *CDK4* gains and losses of *CDKN2A/B* and *BCOR* (42). Transcriptome analysis has also identified two subgroups (stem-like and proinflammatory), with drug assays suggesting that protease inhibitors may be effective in the proinflammatory subgroup (42). It highlights the need for further studies of these biological and molecular alterations, occurring at the time of and after treatment. Better risk stratification is also needed for those most vulnerable and earlier identification for patients who have been treated for a childhood cancer (including non-CNS tumors), potentially with the use of screening during their TYA years. Avoiding the harmful use of radiotherapy to treat childhood cancers should be the goal (43).

A cohort of 207 cases represents one of the largest cohorts of TYA cases published in the literature. However, a limitation of this study is that some of the rarer subgroups identified within this set comprise very small numbers and with limited clinical annotations. Where material is available (and after the provision of molecular testing has been considered), additional IHC studies may be helpful, particularly for novel subgroups, and may assist the neuropathologist in identifying these cases at an earlier stage in the diagnostic workflow, particularly neuropathologists working in lower–middle-income countries. This study also showcases the value of detailed molecular profiling of all HGG cases, irrespective of age, so that we can identify examples of these different tumor types which may be occurring outside of their typical or expected age ranges; this is, and will become, more valuable when further targeted treatments are developed, which are specific to the alterations we see in these cases. For example, hypermutant cases may be eligible for treatment with check point inhibitors (44), and the use of *PDGFRA* (45–47) and MAPK pathway inhibitors (48, 49) are now more established. Other frequently occurring alterations which this study highlights are *CDKN2A/B* deletions and *PTEN* and *MYCN* alterations; although not specific to HGG, therapies targeting these frequent changes may help to improve outcomes as part of combination therapies. One of the most significant challenges with cohort studies is acquiring clinical and survival data. It is important that these data are available in a more accessible way to researchers to enable direct comparisons between the treatment strategies used and to explore the differences in response. Preclinical studies using patient-derived cell cultures and patient-derived and cell-line derived xenografts are needed to support this work. Establishing robust collaborations with local neurosurgical teams will be important for all teams across the neuro-oncology research network to help meet this urgent need.

The development of new molecular tests and the refinement of existing versions are important to consider. For this study, we have used the most recently updated v12.8 MNP classifier. However, future iterations will be produced, and alternative classifiers made available, which can lead to differences in assignments between different versions. It is hoped that the use of allied molecular tests in addition to DNA methylation profiling, already well established in most centers, will not affect patient safety or outcomes and maintain the desired accuracy of diagnosis. It should also be considered that the current version of the classifier is unpublished and developed using data which are not entirely publicly available; within this study, we have attempted to mitigate these challenges through the direct use of the MNP classifier website (the current classifier methodology in diagnostic practice), the development of our own reference cohort (using publicly available data), but also the use of the t-SNE projections and unsupervised clustering as supplementary tools to visually see the distribution of the subgroups. Until the eventual publication of the classifier, this remains the most robust method we have available. The continual development of such evolving platforms must be encouraged and supported. However, it is important for all clinical teams and researchers to be mindful of such changes to see how existing cohorts are affected and whether these changes may be beneficial for TYA patients with HGG.

Conclusion

HGGs occurring in TYAs, perhaps unsurprisingly, overlap with methylation subgroups in the pediatric and adult age groups. Some entities cluster within the TYA age group, whereas others display peaks close to or involving the TYA age range. Novel methylation-defined classes are a feature of TYA HGGs, some of which show mutational landscapes which may be targetable with immune checkpoint, *PDGFRA*, and MAPK pathway inhibitors. Neuro-oncologists should be cautious in assigning tumor subgroups as "adult-type" or "pediatric-type" as this may influence the level of molecular profiling that will be undertaken in certain clinical centers in relation to the age of the patient. Patients who have previously been treated for a childhood malignancy but then develop a secondary HGG, and also backgrounds of tumor predisposition syndromes, are enriched in the TYA population. DNA methylation profiling and WES/panel sequencing should be performed on each TYA HGG to accurately diagnose and characterize these complex tumors.

Authors' Disclosures

J. Sidpra reports grants and personal fees from Cancer Research UK, grants from Olivia Hodson Foundation, and personal fees from University College London outside the submitted work. D.S. Ziegler reports grants from Accendatech and personal fees from Medison Pharma, Roche, Novartis, Alexion, FivepHusion, Amgen, AstraZeneca, Bayer, and Day One Therapeutics outside the submitted work. T.S. Jacques reports grants from the National Institute for Health and Care Research during the conduct of the study as well as grants from The Brain Tumor Charity, Cancer Research UK, Chan Zuckerberg Initiative, Children with Cancer UK, and Olivia Hodson Cancer Fund and other support from Repath Ltd, Neuropath Ltd, and Neuropathology and Applied Neurobiology outside the submitted work. D. Hargrave reports personal fees and nonfinancial support from Day One Therapeutics and Novartis; grants, personal fees, and nonfinancial support from AstraZeneca; and personal fees from Ipsen and Biodexa outside the submitted work. L. Marshall reports personal fees from Bayer, Eisai, and Merck outside the submitted work. No disclosures were reported by the other authors.

Authors' Contributions

R. Pereira: Conceptualization, data curation, formal analysis, writing–original draft. **A. Mackay:** Data curation, formal analysis, methodology, writing–original draft, writing–review and editing. **Y. Grabovska:** Data curation, investigation, writing–original draft, writing–review and editing. **A. Bradley:** Data curation, writing–review and editing. **T. Bloom:** Data curation, writing–review and editing. **J. Nicoll:** Data curation, writing–review and editing. **D. Boche:** Data curation, writing–review and editing. **J. Procter:** Data curation, writing–review and editing. **M. Maybury:** Data curation, writing–review and editing. **J. Schagen:** Data curation, writing–review and editing. **L. Walker:** Data curation, writing–review and editing. **F. Roncaroli:** Data curation, writing–review and editing. **K. Karabatsou:** Resources, data curation, writing–review and editing. **O. Ogunbiyi:** Resources, data curation, writing–review and editing. **T. van Dalen:** Resources, data curation, writing–review and editing. **J. Sidpra:** Resources, data curation. **S. Rossi:** Data curation, investigation, writing–review and editing. **E. Miele:** Data curation, investigation, writing–review and editing. **D.S. Ziegler:** Data curation, writing–review and editing. **Z. Shi:** Data curation, writing–review and editing. **T.S. Jacques:** Data curation, writing–review and editing. **D. Hargrave:** Data curation, writing–review and editing. **B. Zebian:** Resources, data curation, writing–review and editing. **C. Bleil:** Resources, data curation, writing–review and editing. **J. Yates:** Resources, data curation, writing–review and editing. **E. Norton:**

Resources, data curation, writing–review and editing. **H. Mandeville:** Resources, data curation, writing–review and editing. **A. Creak:** Resources, data curation, writing–review and editing. **L. Welsh:** Resources, data curation, writing–review and editing. **L. Marshall:** Resources, data curation, writing–review and editing. **F. Carceller:** Resources, data curation, writing–review and editing. **S.J. Vaidya:** Data curation, software, writing–review and editing. **Z. Reisz:** Resources, data curation, writing–review and editing. **S. Al-Sarraj:** Resources, data curation, writing–review and editing. **A. Mastronuzzi:** Resources, data curation, writing–review and editing. **A. Carai:** Resources, data curation, writing–review and editing. **M. Vinci:** Resources, data curation, writing–review and editing. **K.M. Kurian:** Resources, data curation, writing–review and editing. **H.-k. Ng:** Data curation, software, writing–review and editing. **S. Brandner:** Resources, data curation, writing–review and editing. **C. Jones:** Conceptualization, resources, supervision, funding acquisition, writing–original draft, writing–review and editing. **M. Clarke:** Conceptualization, data curation, formal analysis, funding acquisition, methodology, writing–original draft, project administration, writing–review and editing.

Acknowledgments

D. Hargrave is supported by funding from the National Institute for Health and Care Research Great Ormond Street Hospital Biomedical Research Centre. The Jones Lab is supported by funding from the Royal Marsden Hospital NHS Foundation Trust Biomedical Research Centre, Cancer Research UK, CRIS Cancer Foundation, and the Ollie Young Foundation. The views expressed are those of the author(s) and not necessarily those of the National Health Service, the National Institute for Health and Care Research, or the Department of Health. M. Vinci acknowledges Alfredo Cerimele for technical assistance. 2022 to 2024. Starter Grant for Clinical Lecturers. "The classification and characterization of HGGs in TYAs." 2-year duration. £30,000 over 2 years. Academy of Medical Sciences. 2022 to 2024. Clinical Lecturer Support Grant. "The classification and characterization of HGGs in TYAs." 2-year duration. £100,000 over 2 years. Jean Shanks/Pathological Society of Great Britain. 2022 to 2023. Small Grant Scheme. "The classification and characterization of HGGs in TYAs." 1 year duration. £5000. British Neuropathological Society. 2021 to 2022. Fergus Scholefield Cancer Research Fund. "The classification and characterization of HGGs in TYAs." 1 year duration. £5,000. Penguins Against Cancer. Funding support was also provided by Cancer Research UK (DRCRPG-Nov21/100002), CRIS Cancer Foundation, and the Ollie Young Foundation.

Note

Supplementary data for this article are available at Clinical Cancer Research Online (http://clincancerres.aacrjournals.org/).

Received April 19, 2024; revised September 30, 2024; accepted March 5, 2025; posted first March 10, 2025.

References

1. Guerreiro Stucklin AS, Ryall S, Fukuoka K, Zapotocky M, Lassaletta A, Li C, et al. Alterations in ALK/ROS1/NTRK/MET drive a group of infantile hemispheric gliomas. Nat Commun 2019;10:4343.
2. Clarke M, Mackay A, Ismer B, Pickles JC, Tatevossian RG, Newman S, et al. Infant high-grade gliomas comprise multiple subgroups characterized by novel targetable gene fusions and favorable outcomes. Cancer Discov 2020;10:942–63.
3. Ostrom QT, Cioffi G, Gittleman H, Patil N, Waite K, Kruchko C, et al. CBTRUS statistical report: primary brain and other central nervous system tumors diagnosed in the United States in 2012–2016. Neuro Oncol 2019;21:V1–100.
4. Giangaspero F, Gianno F, Antonelli M, Ferretti E, Massimino M, Arcella A. Pediatric high-grade glioma: a heterogeneous group of neoplasms with different molecular drivers. Glioma 2018;1:117.
5. Ostrom QT, Cote DJ, Ascha M, Kruchko C, Barnholtz-Sloan JS. Adult glioma incidence and survival by race or ethnicity in the United States from 2000 to 2014. JAMA Oncol 2018;4:1254–62.
6. Rong L, Li N, Zhang Z. Emerging therapies for glioblastoma: current state and future directions. J Exp Clin Cancer Res 2022;41:142.
7. Pollack IF, Agnihotri S, Broniscer A. Childhood brain tumors: current management, biological insights, and future directions. J Neurosurg Pediatr 2019;23:261–73.
8. Capper D, Jones DTW, Sill M, Hovestadt V, Schrimpf D, Sturm D, et al. DNA methylation-based classification of central nervous system tumours. Nature 2018;555:469–74.
9. Capper D, Stichel D, Sahm F, Jones DTW, Schrimpf D, Sill M, et al Practical implementation of DNA methylation and copy-number-based CNS tumor diagnostics: the Heidelberg experience. Acta Neuropathol 2018;136:181–210.
10. Drexler R, Brembach F, Sauvigny J, Ricklefs FL, Eckhardt A, Bode H, et al. Unclassifiable CNS tumors in DNA methylation-based classification: clinical challenges and prognostic impact. Acta Neuropathol Commun 2024;12:9.
11. Karimi S, Zuccato JA, Mamatjan Y, Mansouri S, Suppiah S, Nassiri F, et al. The central nervous system tumor methylation classifier changes neuro-oncology practice for challenging brain tumor diagnoses and directly impacts patient care. Clin Epigenetics 2019;11:185.
12. Louis DN, Perry A, Wesseling P, Brat DJ, Cree IA, Figarella-Branger D, et al. The 2021 WHO classification of tumors of the central nervous system: a summary. Neuro Oncol 2021;23:1231–51.
13. Gianno F, Giovannoni I, Cafferata B, Diomedi-Camassei F, Minasi S, Barresi S, et al. Paediatric-type diffuse high-grade gliomas in the 5th CNS WHO Classification. Pathologica 2022;114:422–35.
14. Alken SP, D'Urso P, Saran FH. Managing teenage/young adult (TYA) brain tumors: a UK perspective. CNS Oncol 2015;4:235–46.
15. Roux A, Pallud J, Saffroy R, Edjlali-Goujon M, Debily M-A, Boddaert N, et al. High-grade gliomas in adolescents and young adults highlight histomolecular differences from their adult and pediatric counterparts. Neuro Oncol 2020;22:1190–202.
16. Mackay A, Burford A, Carvalho D, Izquierdo E, Fazal-Salom J, Taylor KR, et al. Integrated molecular meta-analysis of 1,000 pediatric high-grade and diffuse intrinsic pontine glioma. Cancer Cell 2017;32:520–37.e5.
17. Gottardo NG, Gajjar A. Chemotherapy for malignant brain tumors of childhood. J Child Neurol 2008;23:1149–59.
18. Terziev R, Psimaras D, Marie Y, Feuvret L, Berzero G, Jacob J, et al. Cumulative incidence and risk factors for radiation induced leukoencephalopathy in high grade glioma long term survivors. Sci Rep 2021;11:10176.
19. Wu J, Heidelberg RE, Gajjar A. Adolescents and young adults with cancer: CNS tumors. J Clin Oncol 2024;42:686–95.
20. da Costa MDS, Camargo NC, Dastoli PA, Nicácio JM, Benevides Silva FA, Sucharski Figueiredo ML, et al. High-grade gliomas in children and adolescents: is there a role for reoperation? J Neurosurg Pediatr 2020;27:160–9.
21. Mackay A, Burford A, Molinari V, Jones DTW, Izquierdo E, Brouwer-Visser J, et al. Molecular, pathological, radiological, and immune profiling of non-brainstem pediatric high-grade glioma from the HERBY phase II randomized trial. Cancer Cell 2018;33:829–42.e5.
22. Specialist cancer services for children and young people: teenage and young adults designated Hospitals. 2023. Available from: https://www.england.nhs.uk/publication/specialistcancer-services-for-children-and-young-people-teenage-and-young-adults-designated-hospitals/.
23. Nicoll JAR, Bloom T, Clarke A, Boche D, Hilton D. Brain UK: accessing NHS tissue archives for neuroscience research. Neuropathol Appl Neurobiol 2022;48:e12766.
24. Sturm D, Orr BA, Toprak UH, Hovestadt V, Jones DTW, Capper D, et al. New brain tumor entities emerge from molecular classification of CNS-PNETs. Cell 2016;164:1060–72.
25. Sturm D, Capper D, Andreiuolo F, Gessi M, Kölsche C, Reinhardt A, et al. Multiomic neuropathology improves diagnostic accuracy in pediatric neuro-oncology. Nat Med 2023;29:917–26.
26. Gritsch S, Batchelor TT, Gonzalez Castro LN. Diagnostic, therapeutic, and prognostic implications of the 2021 World Health Organization classification of tumors of the central nervous system. Cancer 2022;128:47–58.
27. Ferrari A, Stark D, Peccatori FA, Fern L, Laurence V, Gaspar N, et al. Adolescents and young adults (AYA) with cancer: a position paper from the AYA Working Group of the European Society for Medical Oncology (ESMO) and the European Society for Paediatric Oncology (SIOPE). ESMO Open 2021;6:100096.

28. Reinhardt A, Stichel D, Schrimpf D, Koelsche C, Wefers AK, Ebrahimi A, et al. Tumors diagnosed as cerebellar glioblastoma comprise distinct molecular entities. Acta Neuropathol Commun 2019;7;163.
29. Hansford JR, Das A, McGee RB, Nakano Y, Brzezinski J, Scollon SR, et al. Update on cancer predisposition syndromes and surveillance guidelines for childhood brain tumors. Clin Cancer Res 2024;30:2342–50.
30. Michaeli O, Tabori U. Pediatric high grade gliomas in the context of cancer predisposition syndromes. J Korean Neurosurg Soc 2018;61:319–32.
31. Choi S, Yu Y, Grimmer MR, Wahl M, Chang SM, Costello JF. Temozolomide-associated hypermutation in gliomas. Neuro Oncol 2018;20:1300–9.
32. Hadad S, Gupta R, Oberheim Bush NA, Taylor JW, Villanueva-Meyer JE, Young JS, et al. "De novo replication repair deficient glioblastoma, IDH-wildtype" is a distinct glioblastoma subtype in adults that may benefit from immune checkpoint blockade. Acta Neuropathol 2023;147:3.
33. Das A, Ercan AB, Tabori U. An update on central nervous system tumors in germline replication-repair deficiency syndromes. Neurooncol Adv 2024;6:vdae102.
34. Das A, Fernandez NR, Levine A, Bianchi V, Stengs LK, Chung J, et al. Combined immunotherapy improves outcome for replication-repair-deficient (RRD) high-grade glioma failing anti-PD-1 monotherapy: a report from the international RRD consortium. Cancer Discov 2024;14:258–73.
35. Touat M, Li YY, Boynton AN, Spurr LF, Iorgulescu JB, Bohrson CL, et al. Mechanisms and therapeutic implications of hypermutation in gliomas. Nature 2020;580:517–23.
36. Ilencikova D, Sejnova D, Jindrova J, Babal P. High-grade brain tumors in siblings with biallelic MSH6 mutations. Pediatr Blood Cancer 2011;57:1067–70.
37. Carret A-S, Tabori U, Crooks B, Hukin J, Odame I, Johnston DL, et al. Outcome of secondary high-grade glioma in children previously treated for a malignant condition: a study of the Canadian Pediatric Brain Tumour Consortium. Radiother Oncol 2006;81:33–8.
38. Maluf FC, DeAngelis LM, Raizer JJ, Abrey LE. High-grade gliomas in patients with prior systemic malignancies. Cancer 2002;94:3219–24.
39. Deng MY, Sturm D, Pfaff E, Sill M, Stichel D, Balasubramanian GP, et al. Radiation-induced gliomas represent H3-/IDH-wild type pediatric gliomas with recurrent PDGFRA amplification and loss of CDKN2A/B. Nat Commun 2021;12:5530.
40. Whitehouse JP, Howlett M, Federico A, Kool M, Endersby R, Gottardo NG. Defining the molecular features of radiation-induced glioma: a systematic review and meta-analysis. Neurooncol Adv 2021;3:vdab109.
41. López GY, Van Ziffle J, Onodera C, Grenert JP, Yeh I, Bastian BC, et al. The genetic landscape of gliomas arising after therapeutic radiation. Acta Neuropathol 2019;137:139–50.
42. DeSisto J, Lucas JT Jr, Xu K, Donson A, Lin T, Sanford B, et al. Comprehensive molecular characterization of pediatric radiation-induced high-grade glioma. Nat Commun 2021;12:5531.
43. Jeha S, Pei D, Choi J, Cheng C, Sandlund JT, Coustan-Smith E, et al. Improved CNS control of childhood acute lymphoblastic leukemia without cranial irradiation: St Jude Total Therapy Study 16. J Clin Oncol 2019;37:3377–91.
44. Bouffet E, Larouche V, Campbell BB, Merico D, de Borja R, Aronson M, et al. Immune checkpoint inhibition for hypermutant glioblastoma multiforme resulting from germline biallelic mismatch repair deficiency. J Clin Oncol 2016;34:2206–11.
45. Yang W, Wang S, Zhang X, Sun H, Zhang M, Chen H, et al. New natural compound inhibitors of PDGFRA (platelet-derived growth factor receptor α) based on computational study for high−grade glioma therapy. Front Neurosci 2023;16:1060012.
46. Lane R, Cilibrasi C, Chen J, Shah K, Messuti E, Mazarakis NK, et al. PDGF-R inhibition induces glioblastoma cell differentiation via DUSP1/p38^{MAPK} signalling. Oncogene 2022;41:2749–63.
47. Paugh BS, Zhu X, Qu C, Endersby R, Diaz AK, Zhang J, et al. Novel oncogenic PDGFRA mutations in pediatric high-grade gliomas. Cancer Res 2013;73:6219–29.
48. Stitzlein LM, Adams JT, Stitzlein EN, Dudley RW, Chandra J. Current and future therapeutic strategies for high-grade gliomas leveraging the interplay between epigenetic regulators and kinase signaling networks. J Exp Clin Cancer Res 2024;43:12.
49. Izquierdo E, Carvalho DM, Mackay A, Temelso S, Boult JKR, Pericoli G, et al. DIPG harbors alterations targetable by MEK inhibitors, with acquired resistance mechanisms overcome by combinatorial inhibition. Cancer Discov 2022;12:712–29.